

# SCIENTIFIC REPORTS

OPEN

## Trapping of ivermectin by a pentameric ligand-gated ion channel upon open-to-closed isomerization

Nurit Degani-Katzav, Moshe Klein, Moran Har-Even, Revital Gortler, Ruthi Tobi & Yoav Paas

Received: 05 August 2016

Accepted: 11 January 2017

Published: 20 February 2017

Ivermectin (IVM) is a broad-spectrum anthelmintic drug used to treat human parasitic diseases like river blindness and lymphatic filariasis. By activating invertebrate pentameric glutamate-gated chloride channels (GluCl receptors; GluClRs), IVM induces sustained chloride influx and long-lasting membrane hyperpolarization that inhibit neural excitation in nematodes. Although IVM activates the *C. elegans* heteromeric GluCl $\alpha/\beta$  receptor, it cannot activate a homomeric receptor composed of the *C. elegans* GluCl $\beta$  subunits. To understand this incapability, we generated a homopentameric  $\alpha 7$ -GluCl $\beta$  chimeric receptor that consists of an extracellular ligand-binding domain of an  $\alpha 7$  nicotinic acetylcholine receptor known to be potentiated by IVM, and a chloride-selective channel domain assembled from GluCl $\beta$  subunits. Application of IVM prior to acetylcholine inhibited the responses of the chimeric  $\alpha 7$ -GluCl $\beta$ R. Adding IVM to activated  $\alpha 7$ -GluCl $\beta$ Rs, considerably accelerated the decline of ACh-elicited currents and stabilized the receptors in a non-conducting state. Determination of IVM association and dissociation rate constants and recovery experiments suggest that, following initial IVM binding to open  $\alpha 7$ -GluCl $\beta$ Rs, the drug induces a conformational change and locks the ion channel in a closed state for a long duration. We further found that IVM also inhibits the activation by glutamate of a homomeric receptor assembled from the *C. elegans* full-length GluCl $\beta$  subunits.

Ivermectin (IVM) is a macrocyclic lactone widely used as an anthelmintic drug to treat filarial diseases like onchocerciasis (river blindness) and elephantiasis (lymphatic filariasis) that afflict hundreds of millions of people worldwide<sup>1,2</sup>. IVM is also broadly used in cattle, swine and pets to kill gastrointestinal roundworms, lungworms, grubs, sucking lice and mange mites<sup>3</sup>. The high efficiency of IVM stems from its capability to activate invertebrate glutamate (Glu)-gated chloride channels (GluCl receptors; GluClRs) at nanomolar concentrations, and to keep the receptor's ion channel continuously open<sup>4–9</sup>. Since the GluClRs are chloride selective, IVM causes sustained hyperpolarization across postsynaptic membranes, which inhibits vital functions in the worm like, locomotion<sup>10</sup>, pharyngeal muscle activity<sup>11–13</sup> and secretion processes crucial for evading the host immune system<sup>14</sup>; reviewed by Geary and Moreno<sup>15</sup> and Wolstenholme<sup>16</sup>.

GluClRs are pentamers belonging to the Cys-loop receptor superfamily<sup>17</sup>. As such, they share high primary, secondary, tertiary and quaternary structural homologies with other cationic or anionic Cys-loop receptors whose activating neurotransmitters are acetylcholine (ACh)<sup>18–27</sup>, serotonin<sup>28,29</sup>,  $\gamma$ -aminobutyric acid (GABA)<sup>30–33</sup>, glycine (Gly)<sup>34–40</sup> or histamine<sup>41–43</sup>. Noteworthy, IVM can activate and/or potentiate a few vertebrate Cys-loop receptors, like GABA- and Gly-activated Cl<sup>−</sup> channels<sup>43–53</sup>, and the  $\alpha 7$ -nicotinic AChR<sup>54,55</sup>, as well as the P2X ATP-gated ion channels<sup>56–59</sup>, though with much higher concentrations than in GluClRs.

Genes (*glc-1* and *glc-2*) encoding two GluClR homologous subunits, GluCl $\alpha$  (GLC-1; also named GluCl $\alpha 1$ ) and GluCl $\beta$  (GLC-2), were firstly cloned from the non-parasitic nematode *C. elegans*<sup>4</sup>. Later, additional genes encoding subunits of Glu-gated chloride channels were cloned from *C. elegans*<sup>60</sup> and other invertebrates<sup>61</sup> like parasitic worms<sup>62–65</sup>, insects<sup>66–71</sup>, crustaceans<sup>72</sup>, and mollusk<sup>73</sup>. In several cases, a single subunit was found to form a functional homomeric receptor-channel that can be gated by both Glu and IVM independently. For example, the GluCl $\alpha 2$  (AVR-15) subunit of *C. elegans*<sup>6</sup>, the DrosGluCl- $\alpha$  subunit of *Drosophila melanogaster*<sup>74</sup>,

Laboratory of Ion Channels, The Mina and Everard Goodman Faculty of Life Sciences and The Institute of Nanotechnology and Advanced Materials, Bar-Ilan University, Ramat Gan 52900, Israel. Correspondence and requests for materials should be addressed to Y.P. (email: yoav.paas@biu.ac.il)

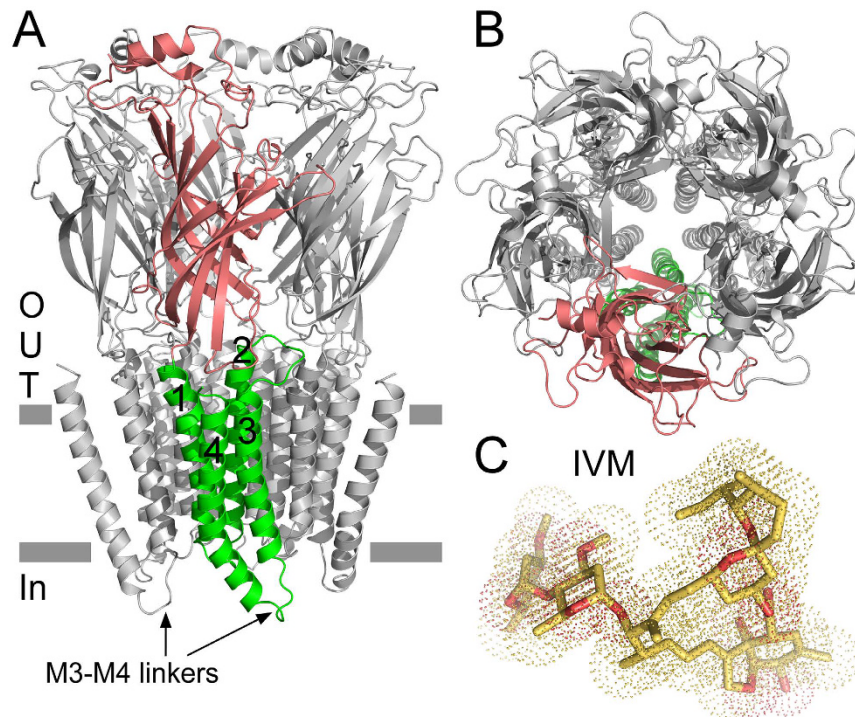


**Figure 1. Structural properties of the chimeric  $\alpha 7$ -GluCl $\beta 3$ R.** (A) Side view of a three-dimensional (3-D) homology model of the chimeric  $\alpha 7$ -GluCl $\beta 3$ R. For clarity, one of the five subunits is colored as follows. The N-terminal segment (reddish) forms the extracellular ligand-binding domain upon receptor assembly. The C-terminal segment (green) has four transmembrane helices (numbered 1 to 4) and it forms the ion-channel pore domain upon receptor assembly. The M3–M4 linkers of two adjacent subunits are indicated; they are much longer in the experimented receptor, but their structure is missing, as it is unavailable in the atomic-scale template used for homology modelling. (B) Top view of the  $\alpha 7$ -GluCl $\beta 3$ R homology model showing five identical subunits, organized in a five-fold symmetry around the axis of ion conduction that is perpendicular to the viewer. (C) Three dimensional structure of ivermectin. Carbon and oxygen atoms are colored in yellow and red, respectively.

the GluCl $\alpha 2\beta$  subunit of *H. contortus*<sup>75</sup>, the MdGluCl $\alpha$  subunit of *Musca domestica*<sup>66</sup>, the GluCl exon-3 variants of *Bombyx mori*<sup>68</sup>, and the AgGluCl-a1 of *Anopheles gambiae*<sup>70</sup>. In contrast, when expressed in *Xenopus* oocytes, the *C. elegans* GluCl $\alpha$  subunit (GLC-1) forms homomeric receptors that can be activated by IVM but not by Glu, whereas the *C. elegans* GluCl $\beta$  subunit (GLC-2) forms homomeric receptors that can be activated by Glu but not by IVM<sup>4,7,8,76</sup>. On the other hand, a heteromeric GluClR consisting of the *C. elegans*  $\alpha$  (GLC-1) and  $\beta$  (GLC-2) subunits can be activated by both Glu and IVM independently<sup>4–9</sup>.

A three-dimensional (3-D) crystal structure of a truncated homomeric GluCl $\alpha$  receptor (GluCl $\alpha_{\text{crist}}$ , PDB 3RIF) indicates that IVM binds at the  $\alpha/\alpha$  intersubunit interfaces in the ion-channel pore periphery<sup>77</sup>. A recent study indicates that incorporation of the GluCl $\beta$  subunit in *C. elegans* GluClR assemblies confers increased receptor sensitivity to IVM<sup>78</sup>. Taken together with a recent determination of the subunit stoichiometry and arrangement in a *C. elegans* heteromeric GluCl $\alpha/\beta$ R<sup>79</sup>, it seems reasonable that IVM binds at GluCl  $\beta/\alpha$  intersubunit interfaces. So, if IVM can interact with the GluCl $\beta$  subunit to activate the *C. elegans* heteromeric GluCl $\alpha/\beta$ R, then why can it not activate the homomeric GluCl $\beta$ R? To answer this question, we have first analyzed the effects of IVM on a highly expressed chimeric  $\alpha 7$ -GluCl $\beta 3$ R whose extracellular ligand-binding domain binds ACh to gate a transmembrane ion-channel pore adopted from the *C. elegans* GluCl $\beta 3$ R. Subsequently, we determined the effect of IVM on homomeric receptors assembled from the full-length *C. elegans* GluCl $\beta 3$  subunit.

## Results

**Structural and basic functional properties of the chimeric  $\alpha 7$ -GluCl $\beta 3$  receptor.** In this study, we have used a chimeric Cys-loop receptor that consists of five identical subunits. Each subunit is a chimera generated by fusing the N-terminal extracellular sequence of the neuronal  $\alpha 7$  nicotinic acetylcholine receptor ( $\alpha 7$ -nAChR) subunit to the C-terminal transmembrane and intracellular sequence of the *C. elegans* GluCl $\beta 3$  subunit (GLC-2) (Supplementary Fig. S1)<sup>80,81</sup>. This chimeric  $\alpha 7$ -GluCl $\beta 3$  Cys-loop receptor robustly responds to ACh that binds to the extracellularly facing ligand-binding domain (LigBD) to open a Cl<sup>-</sup>-selective ion channel pore<sup>80,81</sup>. Figure 1A and B, presents a homology model of the chimeric  $\alpha 7$ -GluCl $\beta 3$ R. Figure 1C depicts a 3-D structure of IVM.

Figure 2 shows representative ACh-evoked currents and a dose-response curve indicating an ACh-EC<sub>50</sub> value of  $46 \pm 14 \mu\text{M}$  and a Hill coefficient of  $2.55 \pm 0.3$ . These values are very close to previous determinations<sup>81</sup>.

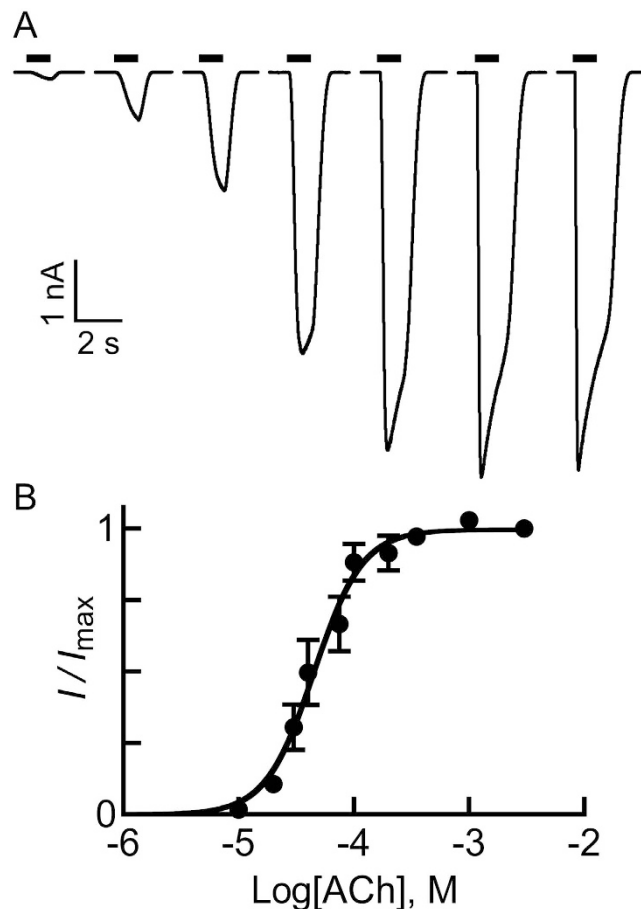


**Figure 2. ACh-activation properties of the chimeric  $\alpha 7$ -GluCl $\beta$ R.** (A) Representative current traces evoked by ACh in Chinese hamster ovary (CHO) cells expressing the chimeric  $\alpha 7$ -GluCl $\beta$ R. ACh was applied for 1 sec at micromolar concentrations of: 10, 20, 30, 75, 200, 1000 and 3000 (black bars). Recordings were performed at  $-60$  mV. (B) A dose-response curve plotted for the responses of the  $\alpha 7$ -GluCl $\beta$ R to ACh. Data was extracted from experiments performed as in panel A. The curve was fitted to the averaged data points with a non-linear regression using the Hill equation 1 (Eq. 1, see “Materials and Methods”) ( $r^2 = 0.996$ ). Error bars correspond to SEM (N = 12).

**Application of IVM prior to ACh inhibits the responses of the  $\alpha 7$ -GluCl $\beta$ R.** IVM can activate the *C. elegans* homomeric GluCl $\alpha$  and heteromeric GluCl $\alpha/\beta$  receptors expressed either in *Xenopus* oocytes<sup>4–8,61,82</sup>, HEK cells<sup>78</sup> or CHO cells<sup>79</sup>, but it cannot activate the *C. elegans* homomeric GluCl $\beta$ R expressed in these cells<sup>4,7,8,76,78,79</sup>. Since, in the GluCl $\alpha_{\text{crist}}$ R, IVM binds at the periphery of the ion-channel pore domain<sup>77</sup>, we reasoned that IVM would not activate the chimeric  $\alpha 7$ -GluCl $\beta$ R whose ion-channel pore domain is that of the GluCl $\beta$ R. On the other hand, previous studies performed with the  $\alpha 7$ -nAChR showed that IVM potentiated the ACh-elicited currents and decreased the ACh-EC<sub>50</sub> by 20 fold<sup>54,55</sup>. Hence, we were wondering whether IVM would be able to potentiate the response of the chimeric  $\alpha 7$ -GluCl $\beta$ R to ACh. Our curiosity emerged since, in the GluCl $\alpha_{\text{crist}}$ R, IVM forms a few van der Waals interactions with the M2-M3 loop<sup>77</sup> that is located at the interface between the LigBD and the pore domain and interacts with entities of the LigBD to gate Cys-loop receptors. For example, in the GABA<sub>A</sub>R<sup>83–85</sup>, GlyR<sup>86,87</sup>, 5HT<sub>3A</sub>R<sup>88–90</sup>, muscle nAChR<sup>91–93</sup>, neuronal  $\alpha 7$ -nAChR<sup>94–96</sup>, as well as in the chimeric  $\alpha 7$ -GlyR<sup>97</sup> and  $\alpha 7$ -5HT<sub>3A</sub>R<sup>98</sup>.

Figure 3 shows robust responses to ACh alone ( $I_{p1}$ ) or to ACh applied immediately after pre-application of 0.01% DMSO (the content in the IVM-containing solution) ( $I_{p2}$ ). The DMSO-containing solution had no significant effect on the current amplitude ( $I_{p2}/I_{p1}$  of  $95 \pm 1.8\%$ ;  $P > 0.05$ , N = 42, paired, two-tailed Student’s *t*-tests). In contrast, pre-application of 5  $\mu$ M IVM for 10 sec reduced the ACh-elicited response to  $16 \pm 5.2\%$  of the response obtained immediately after the DMSO pre-application (percent  $I_{p3}/I_{p2}$ ;  $P < 0.001$ , N = 8) (Fig. 3). Notably, the initial responses to ACh could not be recovered even after a long-term wash ( $> 2$  min) (e.g., Fig. 3,  $I_{p4}$ ), and their magnitude was  $4.4 \pm 1.3\%$  of the responses obtained after the DMSO pre-application (percent  $I_{p4}/I_{p2}$ ;  $P < 0.001$ , N = 5).

Since the ACh-evoked response could not be recovered after exposure of the cell to IVM, we had to perform the above application protocol in different cells for each IVM concentration separately. By that, we obtained the inhibition graph shown in the inset of Fig. 3. The IVM-IC<sub>50</sub> was found to be 156 nM, and the Hill coefficient  $\sim 3$ .

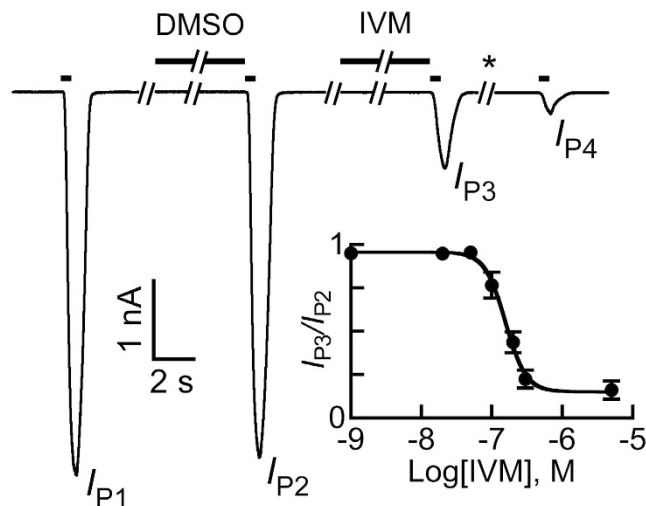


**Figure 3. Inhibitory effect of IVM pre-application on the response of the  $\alpha 7$ -GluCl $\beta$ R to ACh.** Following the first ACh application, which gave peak  $I_{P1}$ , the cell was washed with a physiological solution for 40 sec. Then, as a control, 0.01% DMSO was applied for 10 sec prior to the second ACh application that gave peak  $I_{P2}$ . Next, following a 40-sec-long wash, 5  $\mu$ M IVM (in the presence of 0.01% DMSO) was applied for 10 sec before its replacement by ACh (giving peak  $I_{P3}$ ). Finally, following a 2-min-long wash (\*), ACh was applied again (giving peak  $I_{P4}$ ). In all applications, 50  $\mu$ M ACh was applied for 0.5 seconds. Inset, a curve corresponding to the inhibition of ACh (50  $\mu$ M)-elicited currents by increasing concentrations of IVM. Data were extracted from experiments performed as in panel A. Since the currents could not be recovered following an exposure to IVM, each cell was exposed only to one concentration of IVM. Then, to provide the normalized ACh response, the peak current recorded in response to ACh immediately after IVM application (i.e.,  $I_{P3}$ ) was divided by the peak current recorded in response to ACh immediately after DMSO application (i.e.,  $I_{P2}$ ). The curve was fitted to the averaged data points with a non-linear regression using the Hill equation 2 (Eq. 2;  $r^2 = 0.996$ ). Error bars correspond to SEM. Total of 41 cells were used to obtain the averaged points. Recordings were performed at  $-60$  mV.

The results in Fig. 3 may indicate that IVM binds to the resting (closed) state and cannot dissociate from the receptor during the application of ACh. We however cannot exclude the possibility that the immediate application of ACh after the application of IVM stabilized the receptor in a pre-open state for a long duration. We therefore changed the application protocol and introduced intermediate washes between the IVM and ACh applications. Clearly, neither 5- nor 10-sec-long intermediate washes could prevent the strong inhibitory effect of IVM pre-application ( $I_{P3}$  and  $I_{P3}/I_{P2}$  in Fig. 4A and B, respectively). Furthermore, a long-term wash introduced after the first recovery trial (Fig. 4A, asterisk), was followed by even a greater inhibitory effect ( $I_{P4}$  and  $I_{P4}/I_{P2}$  in Fig. 4A and B, respectively).

Since the GluCl $\alpha_{\text{cryst}}$ R indicates that IVM is accommodated at the protein-lipid interface<sup>77</sup>, we examined the effect of the membrane voltage on the IVM inhibitory effect. Similar effects have been observed at  $-60$  mV and  $-20$  mV (Fig. 4B), suggesting that the electric field of the membrane does not influence IVM association with the chimeric  $\alpha 7$ -GluCl $\beta$ R.

### IVM accelerates the decline of ACh-elicited macroscopic currents in cells expressing $\alpha 7$ -GluCl $\beta$ receptors.

Application of 350  $\mu$ M ACh (saturating concentration) for 5.5 sec on cells expressing the chimeric  $\alpha 7$ -GluCl $\beta$ R, resulted in currents that rapidly reached a peak and then declined to  $31 \pm 8.6\%$  ( $N = 5$ ) of the peak amplitude (Fig. 5A, black trace). We took advantage of the slow and partial current decline observed here, and examined the capability of IVM to associate with the  $\alpha 7$ -GluCl $\beta$ R after activation, during the phase of current decline. To this end, immediately after reaching to the ACh-evoked peak, we added 5  $\mu$ M IVM (dissolved in 0.01% DMSO) to the ACh-containing solution. The red colored current trace in Fig. 5A clearly indicates that IVM accelerates the current decline, and reduces the amplitude of the steady-state current. The grey current trace (Fig. 5A) corresponds to a control showing that 0.01% DMSO does not substantially change the response to ACh alone. Statistical analysis of the time constant of current decline ( $\tau_d$ ) indicates that DMSO alone had no significant effect on  $\tau_d$ , neither at  $-60$  mV nor at  $-20$  mV (Fig. 5B). In contrast, IVM reduced the  $\tau_d$  values by more than two folds at both membrane voltages,  $-60$  mV and  $-20$  mV, to a statistically similar extent (Fig. 5B). These results reinforce our above suggestion that the electric field of the membrane does not influence IVM association with the chimeric  $\alpha 7$ -GluCl $\beta$ R.

**How does IVM decrease Cl $^-$  ion flow through the chimeric  $\alpha 7$ -GluCl $\beta$ R?** The  $\alpha 7$ -nAChR is a fast desensitizing receptor whose current response rapidly declines in the presence of saturating ACh concentrations due to channel closing<sup>96,98-110</sup>. Compared with the  $\alpha 7$ -nAChR, in the case of the chimeric  $\alpha 7$ -GluCl $\beta$ R studied here, the current declines much slower under saturating ACh concentration (e.g., Fig. 5A, black trace). Therefore,

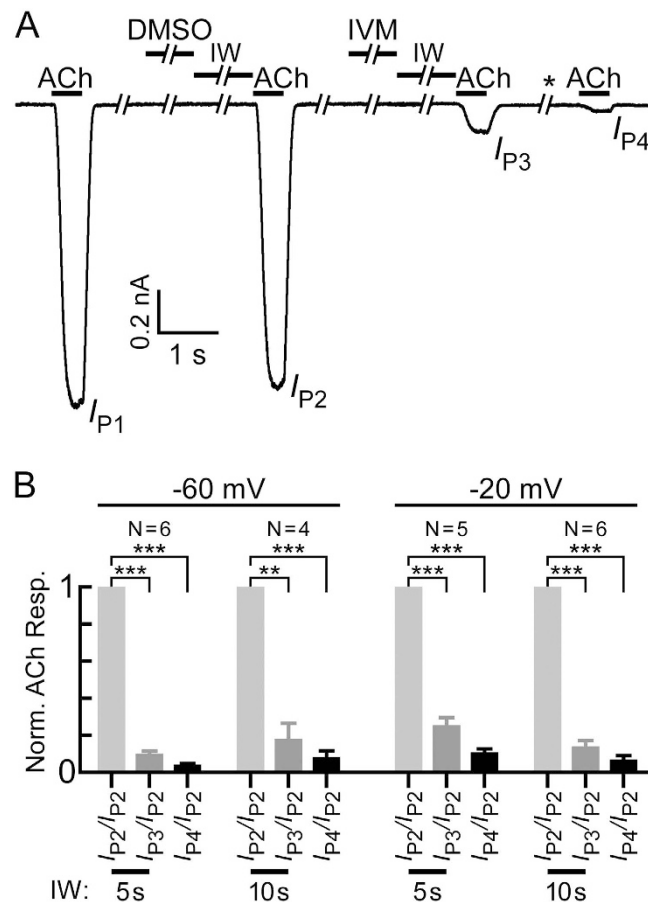


**Figure 4.** Washes introduced between the IVM and ACh applications do not prevent the inhibition by IVM. (A) A representative current trace evoked by ACh to give: a first peak ( $I_{p1}$ ); a second peak ( $I_{p2}$ ) after the DMSO application and an intermediate wash (with a physiological solution, IW); a third peak ( $I_{p3}$ ) after the IVM application and an intermediate wash (IW); and a fourth peak ( $I_{p4}$ ) after further long-term wash ( $* > 100$  sec). In all cases, 50  $\mu$ M ACh was applied for 0.5 seconds. DMSO (0.01%) and IVM (5  $\mu$ M; containing 0.01% DMSO) were applied for 4 seconds. Washes performed immediately after the first and second ACh applications were 40-sec long (not indicated by a bar above the trace). Intermediate washes (IW) were applied for 5 seconds. Recording of this specific trace was performed at  $-60$  mV. (B) Histograms of data extracted from experiments performed as in A, which include a 4-sec-long pre-application of IVM (5  $\mu$ M), followed by a 5- or 10-sec-long intermediate wash (IW) and an ACh (50  $\mu$ M) application (for 0.5 sec), at  $-60$  or  $-20$  mV membrane voltages. Each current peak ( $I_{p3}$  or  $I_{p4}$ ) was normalized to the current peak recorded after the application of 0.01% DMSO ( $I_{p2}$ ) in the same cell (Norm. ACh Resp. stands for normalized acetylcholine response). Each cell was exposed to IVM only once, because the currents could not be recovered even after a long-term wash. The bars correspond to the averaged normalized currents with error bars corresponding to SEM of N cells, as indicated within the figure. The time of the intermediate wash (IW) is indicated at the bottom. Paired, two-tailed Student's *t*-tests indicate that  $***P < 0.0005$  and  $**0.0005 < P < 0.005$ . Two-way analysis of variance (ANOVA) between the  $I_{p3}/I_{p2}$  ratios obtained following 5-sec-long or 10-sec-long intermediate washes, at  $-60$  mV or  $-20$  mV, indicates that there is no difference between the extent of inhibition observed under these four conditions ( $P > 0.05$ ). The same two-way ANOVA probability ( $P > 0.05$ ) was obtained for the  $I_{p4}/I_{p2}$  ratios.

over a relatively long-term recording of inward currents through the  $\text{Cl}^-$ -selective  $\alpha 7$ -GluCl $\beta$ R, the driving force acting on  $\text{Cl}^-$  ions may decrease due to the outflow of  $\text{Cl}^-$  ions and the decrease in their intracellular local concentration near the channels during the recording time window. A decrease in intracellular  $\text{Cl}^-$  ion concentration in the vicinity of the channels has already been suggested for slowly-desensitizing GABA and Gly Cys-loop receptors<sup>111</sup>. To distinguish between desensitization (channel closing) and a decrease in the driving force acting on  $\text{Cl}^-$  ions, we activated the receptors with 30  $\mu$ M ACh, and after the current reached to its peak, we performed voltage ramps throughout the current-declining phase, as has been performed previously<sup>111</sup>. Figure 6A presents an example for such an experiment, where the output currents of the voltage ramps are obtained in the absence of IVM. Superimposition of the voltage-ramps' output currents shows a moderate decrease in slopes (Fig. 6A, right). The current-voltage relations ( $I/V$  curves) extracted from the output currents (Fig. 6C) indicate that, during the application of ACh alone (in the absence of IVM), the reversal potential ( $E_{\text{rev}}$ ) decreases from  $-5.3$  mV to  $-28.9$  mV. The black squares in Fig. 6E correspond to the  $E_{\text{rev}}$  values determined for each voltage ramp when ACh

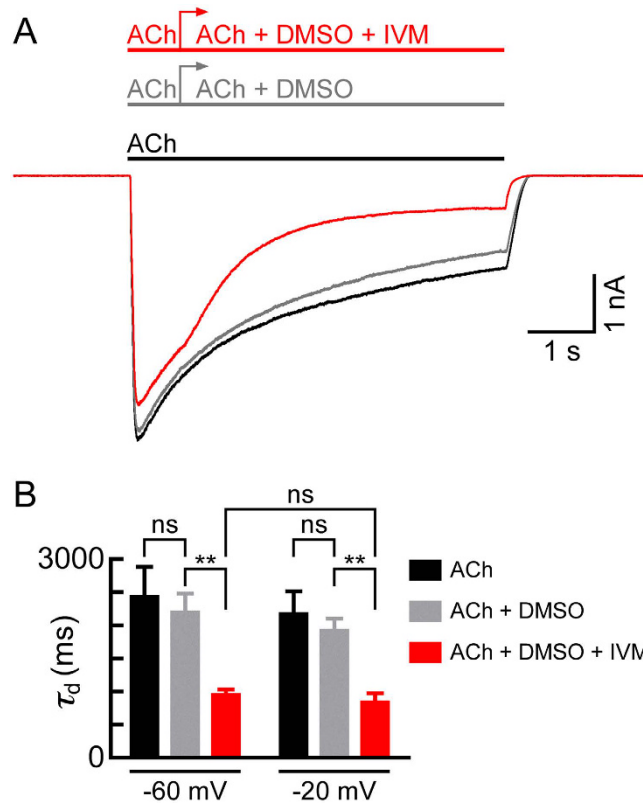


**Figure 5. IVM accelerates the current decline when added after receptor activation by ACh.**

(A) Representative currents elicited first by ACh alone (350  $\mu$ M) that was applied for 5.5 sec (black bar and trace). Following a wash of a minute, the same cell was challenged again with ACh (350  $\mu$ M), and after reaching to the peak (i.e., after 0.75 s), 0.01% DMSO was added, as a control (gray bar, arrow and trace). Following a further wash (for a minute), the same cell was challenged again with a 5- $\mu$ M-IVM solution (in 0.01% DMSO; red bar, arrow and trace). Recordings were performed at  $-60$  mV. (B) Time constant of current decline ( $\tau_d$ ). Values of  $\tau_d$  were determined by exponential fits to the declining phase of the currents using Eq. 3. Data was extracted from experiments performed as in (A) (ACh, 350  $\mu$ M; DMSO, 0.01%; IVM, 5  $\mu$ M). In all three cases, the kinetics was measured at the same time range; starting  $\sim 0.75$  sec after ACh application (the time of DMSO or IVM addition) and ending at the time of wash application. Error bars correspond to SEM of  $N = 6$  and  $N = 5$  cells for recordings at  $-60$  mV and  $-20$  mV, respectively. Paired, two-tailed Student's  $t$ -tests indicate that for not significant ("ns")  $P > 0.3$ , and \*\*  $0.001 < P < 0.005$ .

is applied alone. The leftward (negative) shift in the  $E_{rev}$  values observed in the absence of IVM ( $\Delta E_{rev} = 23.6$  mV; Fig. 6C and E, black squares) reflects a change in the Nernst potential for  $Cl^-$  ions. By using the experimental  $E_{rev}$  values and the Nernst equation (Eq. 4), we calculated the intracellular concentrations of  $Cl^-$  ions ( $[Cl^-]_i$ ) and found that it is 122.7 mM at the beginning and 48.9 mM at the end of the current-decline phase (r1 and r13 in Fig. 6A, respectively). Therefore, when measuring inward  $Cl^-$  currents over 9.6-sec-long applications of ACh alone (e.g., Fig. 6A), a significant component of the current decline can be attributed to a decrease in the electrochemical driving force ( $V_{DF}$ ) acting on  $Cl^-$  ions ( $V_{DF} = V_m - E_{rev}$ ).  $V_{DF}$  probably decreases because  $Cl^-$  ions flow out of the cell, and  $[Cl^-]_i$  in the vicinity of the channels decreases with no capability to recover within the time window of the recording.

We applied the same experimental protocol on the representative cell shown in Fig. 6A, but in the presence of IVM that was added immediately after the current reached to its peak (Fig. 6B). In this experiment, we used 4- $\mu$ M-IVM solution that contained 0.008% DMSO. Superimposition of the voltage ramps' output currents recorded in the presence of IVM shows a sharper decrease in slopes (Fig. 6B, right) than in the absence of IVM (Fig. 6A, right). The  $I/V$  relations indicate that, within the recording time in the presence of IVM, the reversal potential ( $E_{rev}$ ) decreases from  $-7.9$  mV to  $-18.9$  mV (Fig. 6D). The leftward (negative) shift in the reversal potential observed in the presence of IVM ( $\Delta E_{rev} = 11$  mV; Fig. 6D and E, red circles) reflects a much smaller change in the Nernst potential for  $Cl^-$  ions, as compared with the shift observed in the absence of IVM. The  $I/V$  relations allowed us to determine the change in the chloride conductance throughout the 9.6-sec application time. For that, we have calculated the chloride chord conductance at  $-65$  mV (Eq. 5), which turned to be virtually the same as the chloride chord conductance at  $+15$  mV. Figure 6F shows exponential curves fitted to the chord conductance points (Eq. 6) that were calculated from the currents shown in Fig. 6A and B. Clearly, in the presence of 4  $\mu$ M IVM, the chloride conductance declines much faster (red curve) than in the absence of IVM (black curve) (Fig. 6F). Using the experimental  $E_{rev}$  values, we calculated the  $[Cl^-]_i$  and the  $V_{DF}$  for each voltage

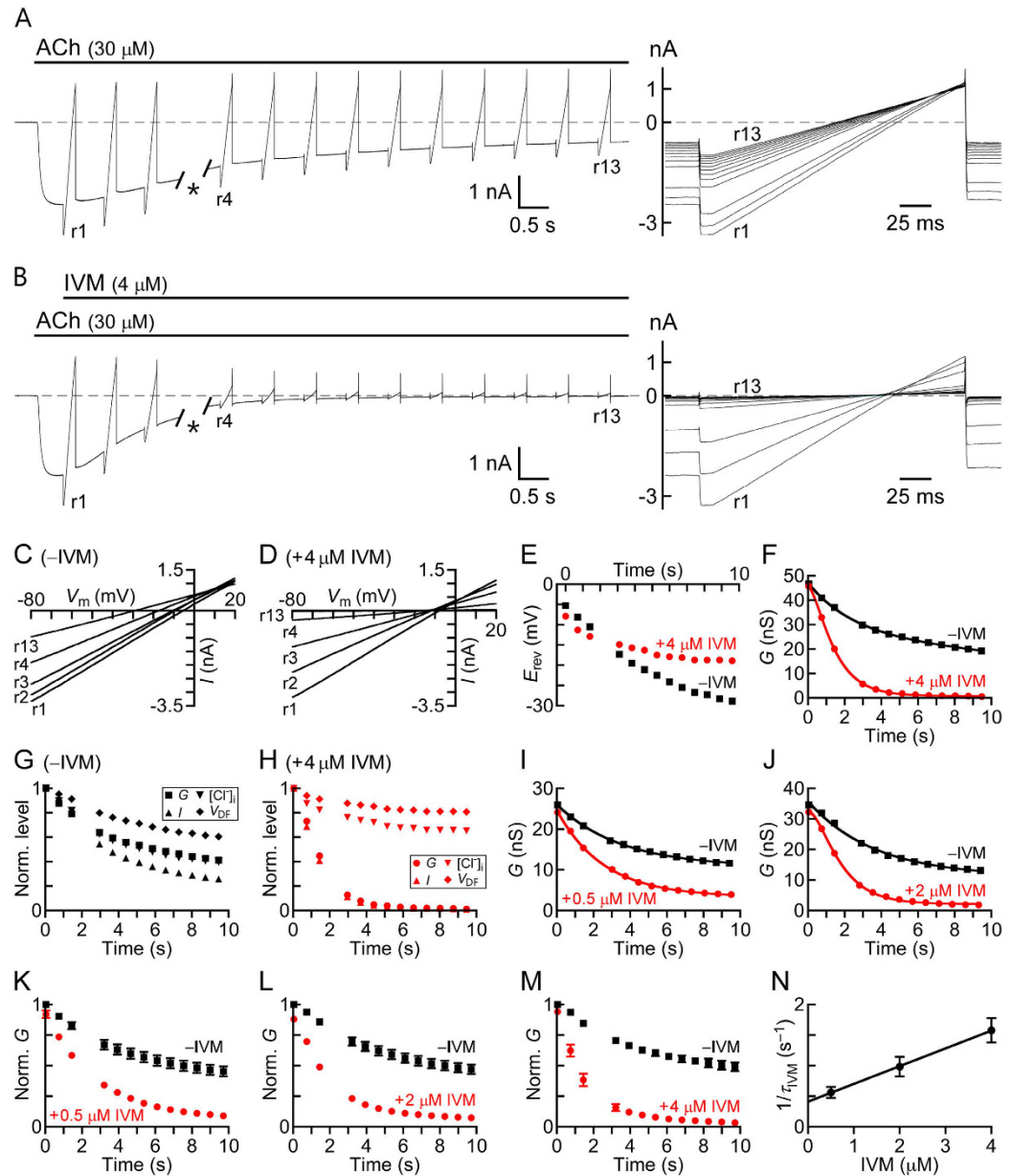


**Figure 6. Chloride conductance of  $\alpha 7$ -GluCl $\beta$ Rs.** Representative whole-cell current traces elicited by: (A) ACh alone and (B) ACh to which IVM was added after the current peak. Recordings were performed at  $-60$  mV with intervening 200-ms-long voltage ramps applied from  $-80$  to  $+20$  mV during the current decline, giving output currents r1–r13. \*, time lapse of  $\sim 1$  sec between protocols' exchange (see "Supplementary Materials and Methods"). Traces in A and B were recorded from the same cell, with an intermediate 74-sec-long wash. Right panels show superimposition of the output currents. (C,D) Current-voltage ( $I/V$ ) relations extracted from A and B, respectively (r13 in D overlaps the x-axis). (E) Reversal potentials ( $E_{rev}$ ) extracted from the voltage-ramps' output currents of A (black squares) and B (red circles), plotted as a function of time (0 sec, time of r1). (F) Decay of chloride chord conductance plotted as a function of time, in the absence or presence of IVM. The conductance points were calculated at  $-65$  mV based on the voltage-ramps' output currents shown in A and B. Exponential fits (Eq. 6) are shown. (G,H) Normalized (Norm.) conductance ( $G$ ), current ( $I$ ), intracellular  $\text{Cl}^-$  ion concentration ( $[\text{Cl}]_i$ ), and electrochemical driving force ( $V_{DF}$ ) plotted as a function of time for ACh-dependent responses in the absence (panel G) or presence (panel H) of IVM (relating to responses in A and B, respectively). (I,J) Decay of chloride chord conductance plotted as a function of time in representative cells exposed to different IVM concentrations. (K,L,M) Averaged normalized chloride chord conductance (Norm.  $G$ ) plotted as a function of time under different IVM concentrations. In each cell, each conductance was normalized to the conductance extracted from r1 of the ACh-alone application.  $N = 7, 11$  and  $8$  in K, L and M, respectively. Error bars are SEM. (N)  $1/\tau_{IVM}$  plotted as a function of IVM concentration, using equation 7 for curve fitting by linear regression ( $r^2 = 0.999$ ). 26 cells were analyzed to obtain the averaged  $1/\tau_{IVM}$  points. Error bars are SEM. In all panels, ACh concentration is  $30 \mu\text{M}$ .

ramp output current at  $-65$  mV, as has been performed above for the ACh application in the absence of IVM. While the changes in  $[Cl]_i$  and  $V_{DF}$  were slower and weaker in the presence of IVM (Fig. 6H) than in the absence of IVM (Fig. 6G), the decline of the conductance and current was much faster and stronger in the presence of IVM (Fig. 6H) than in the absence of IVM (Fig. 6G). Moreover, the current decline and the conductance decline in the presence of IVM overlap. Hence, we suggest that the conductance decline observed in the presence of IVM reflects structural changes in the ion conductance pathway, which eventually prevent  $Cl^-$  ions to cross the ion-channel pore.

To determine the kinetics of conductance decline at lower IVM concentrations we had to use different cells since we could not reproduce the initial robust response (the one shown in Fig. 6A) after the exposure of the cell to IVM, even following a long-term wash (70 seconds) (Supplementary Fig. S2). Figure 6I and J shows the conductance decline in representative cells under IVM concentrations lower than  $4 \mu M$ . The entire analysis described in this section was applied to 26 cells; and the averaged normalized conductance decline, under three different IVM concentrations, is presented in Fig. 6K–M.

We then took advantage of the capability of IVM to accelerate the current decline in order to determine the binding affinity of IVM. To this end, the voltage ramps' output currents obtained in the presence of IVM were subtracted from their counterpart currents obtained in the absence of IVM. Then, we calculated the chloride conductance based on the resulting subtracted currents at each ramp. This chloride conductance is hereafter termed  $G_{IVM}$ . In each experimented cell, we fitted exponential curves to the first 5–6 conductance points, where there was no substantial difference between the  $\Delta E_{rev}$  values in the absence or presence of IVM. These exponential fits for the  $G_{IVM}$  points were obtained at various IVM concentrations, and they actually provide the time constant of the IVM-dependent  $Cl^-$ -conductance decay ( $\tau_{IVM}$ ). Figure 6N shows that the averaged reciprocal  $\tau_{IVM}$  values increase linearly with the increase in IVM concentrations.

IVM does not readily dissociate from the receptor (Supplementary Fig. S2) and the number of possible intermediate IVM-bound states is not known. Hence, the simplest possible kinetic model that could describe the acceleration of current decline in the presence of IVM would be one in which an ACh-activated conducting receptor ( $R^*_{ACh}$ ) closes a gate in the ion-channel pore upon IVM binding ( $IVM \cdot R_{ACh}$ ), as follows:

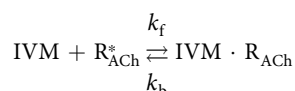
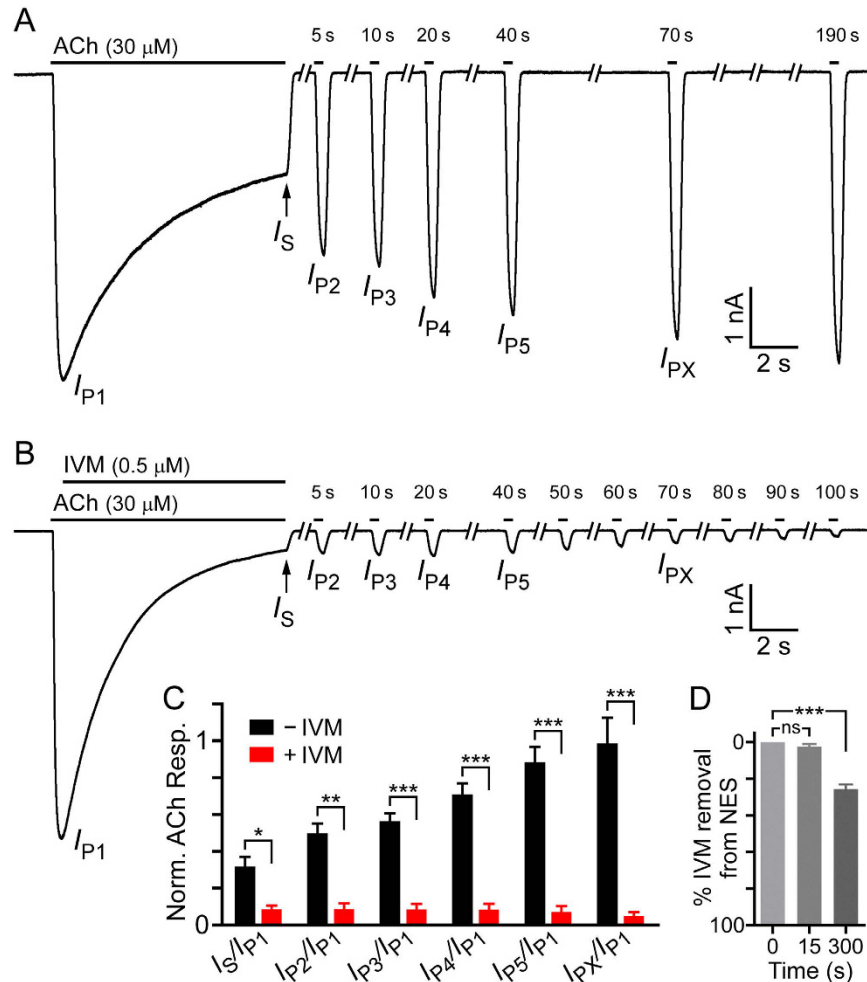


Figure 6N shows a curve fitted to the  $1/\tau_{IVM}$  points by a linear regression using equation 7. The slope of this curve corresponds to the IVM association rate constant ( $k$  forward,  $k_f = 290800 M^{-1} \cdot s^{-1}$ ). The IVM dissociation rate constant ( $k$  backward,  $k_b = 0.41 s^{-1}$ ) is the extrapolated intercept of the linear curve with the y-axis in Fig. 6N. The  $K_d$  ( $k_b/k_f$ ) for IVM binding to an activated  $\alpha 7$ -GluCl $\beta$  chimeric receptor would therefore be  $1.4 \times 10^{-6} M$ . This  $K_d$  value is nine times higher than the  $IC_{50}$  value observed when IVM is applied prior to activation ( $156 nM$ ; Fig. 3).

**IVM becomes trapped during the receptor open-to-closed isomerization.** The residency time for a drug bound to its target is provided by  $1/k_b$ <sup>112</sup>. The results of the previous section indicate that, for IVM, the residency time is  $\sim 2.5$  sec, which means that IVM should have been removed within a wash of a few seconds. However, as said, the initial robust ACh-elicited current response (e.g., Fig. 6A) could not be reproduced following cell exposure to IVM, even after a wash lasting 70 seconds (Supplementary Fig. S2). To better understand the effect of IVM, we applied ACh (alone) for 9.6 seconds and then re-applied the same ACh concentration (alone) several times, each for 350 millisecond. Figure 7A and C (black bars) shows that when re-applications were performed 5, 10, 20 and 40 seconds after the end of the initial (long-term) ACh-application, the current amplitudes did not fully recover. The unrecovered current portion may indicate that the  $[Cl]_i$  near the channels and the  $V_{DF}$  at these time points have not been restored to initial values. We however do not exclude the possibility that part of the current is missing due to acute desensitization<sup>113</sup>, which may result in reversible stabilization of the receptor in a deeply desensitized (closed) state - as has been suggested for nAChRs in midbrain dopamine neurons<sup>114</sup> and recombinant  $\alpha 4\beta 2$  neuronal nicotinic AChRs<sup>115</sup> (reviewed by Giniatullin *et al.*<sup>116</sup>). Figure 7A and C (black bars) also shows that it takes at least 70 seconds for the macroscopic current amplitude to recover. This recovery excludes the possibility of functional rundown since there was no permanent inactivation as described, for example, in recombinant  $\alpha 3\beta 2$ <sup>117</sup>,  $\alpha 4\beta 2$ <sup>118</sup> and  $\alpha 7$ <sup>119</sup> nAChRs. When IVM was combined with ACh after the current reached to its peak in the long-term application, the current amplitude could not be recovered even after 100 sec of wash (Fig. 7B and C, red bars).

To examine if IVM can be removed from the receptor by longer wash periods, we extended the washing time. Figure 8A shows a control experiment, where ACh was applied alone for 9.6 seconds followed by two additional short-term ACh applications (350 milliseconds), with two intermediate washes each lasting 3 minutes. As can be seen in Fig. 8A, the initial (long-term) ACh application resulted in a response that reached a peak ( $I_{p1}$ ) and declined with one exponential time course ( $\tau_{d1}$ , Fig. 8C). The current remaining at the end of the initial ACh application was  $35 \pm 4\%$  of the initial peak (percent  $I_s/I_{p1}$  in Fig. 8D, black bars). Figure 8A and D (black bars) also shows that the initial current amplitude ( $I_{p1}$ ) was completely recovered ( $I_{p3}/I_{p1}$ ). In contrast, when IVM was added to ACh immediately after the current reached to its peak (Fig. 8B, leftmost response), the current declined with double exponential time course. One of the two time constants ( $\tau_{d2}$ ) is significantly smaller than the time constant measured in the presence of ACh alone (Fig. 8C;  $P < 0.0001$ , unpaired, two-tailed Student's *t*-test). In addition, the steady-state current ( $I_s$ ) was found to be  $6\% \pm 0.01\%$  of the initial amplitude, significantly smaller than in ACh alone (Fig. 8D, percent  $I_s/I_{p1}$ , red bar vs black bar). Furthermore, very small responses could be seen upon re-application of ACh alone after 3 and 6 minutes of wash (Fig. 8B, inset; Fig. 8D,  $I_{p2}/I_{p1}$  and  $I_{p3}/I_{p1}$  in red).





**Figure 7. Recovery of ACh-evoked currents in the absence or presence of IVM.** (A) Representative currents elicited by a long-term application (9.6 sec) of  $30\ \mu\text{M}$  ACh to obtain peak  $I_{P1}$ , followed by repetitive short-term applications (350 ms) of  $30\ \mu\text{M}$  ACh (black bars above the current traces) with intermediate washes. Times indicated above the short bars were measured from the end of the initial, long-term ACh application (that gave  $I_{P1}$  and  $I_S$ ). (B) Representative currents for the same experiment as in A, but with IVM ( $0.5\ \mu\text{M}$ ) added after peak  $I_{P1}$ . Currents in A and B were measured at  $-60\ \text{mV}$ . (C) Normalized ACh response (y-axis) calculated by the current peak ratios that are indicated below the x-axis. Current peak ratios were extracted from experiments like those shown in A and B. Black bars correspond to results obtained with ACh alone, as in panel A ( $N=8$ ). Red bars correspond to ACh-elicited currents where IVM was added as in panel B ( $N=5$ ). Error bars correspond to SEM. Asterisks correspond to unpaired, two-tailed Student's  $t$ -tests with  $0.001 < *P < 0.05$ ,  $0.0001 < **P < 0.001$  and  $***P < 0.0001$ . (D) Fractional removal of IVM from the aqueous phase of a 1-ml solutions containing 140,000 CHO cells and  $4\ \mu\text{M}$  IVM. Removal of IVM was determined following the indicated incubation times by measuring the absorbance of supernatants at 245 nm wavelength (e.g., Supplementary Fig. S3; Supplementary Materials and Methods). Note that, no IVM removal is indicated at the top of the y-axis. Mean  $\pm$  SEM of seven independent experiments are presented. Paired, two-tailed Student's  $t$ -tests indicate that for "ns" (not significant)  $P > 0.2$ , and  $***P < 0.0001$ .

Since, in the control experiments, the current could be recovered almost completely after a 3-min wash (Fig. 8A,  $I_{P2}$ ; Fig. 8D,  $I_{P2}/I_{P1}$  in black), we conclude that the  $[\text{Cl}]_i$  in the vicinity of the channels and  $V_{DF}$  largely recovered within the 3-min wash. When IVM is added, the recovery of the  $[\text{Cl}]_i$  and  $V_{DF}$  is expected to take place even sooner, because compared with the control, the current declines much faster to  $I_S$  and  $I_S/I_{P1}$  is much lower (Fig. 8A vs B; Fig. 8C and D,  $I_S/I_{P1}$ , black vs red bars). Hence, the incapability of ACh to elicit currents after exposure to IVM (Fig. 8B,  $I_{P2}$  and  $I_{P3}$ ; Fig. 8D,  $I_{P2}/I_{P1}$  and  $I_{P3}/I_{P1}$  in red) strongly indicates that IVM stabilizes, for a long duration, a channel state having an obstructed ion-conduction pathway.

#### Does IVM accumulate in the CHO cell plasma membrane during the time of its application?

The capability of a fluorescent ivermectin probe to partition into biological membranes and diffuse laterally in the lipid bilayer was previously demonstrated following its incubation for 30 minutes with muscle vesicle membranes prepared from the parasite *Ascaris sum*<sup>120</sup>. The lipophilic properties of IVM were also demonstrated by incubating

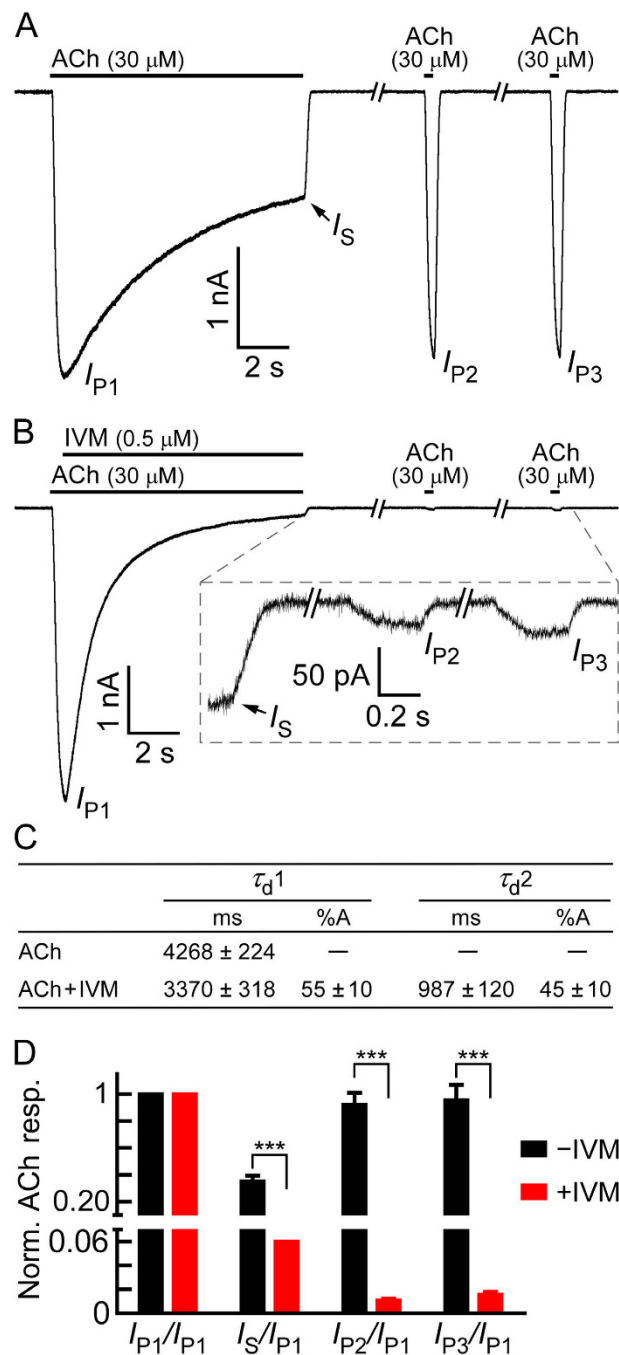


**Figure 8. The inhibition of ACh-elicited currents by addition of IVM is irreversible.** (A) Representative currents elicited by a long-term application (9.6 sec) of ACh followed by two short-term (350 ms) applications of ACh, with intermediate long-term washes, each lasting 3 minutes. (B) Representative currents for the same experiment as in A, but with the exception of IVM (0.5  $\mu$ M) addition after the ACh-elicited current reached to its peak ( $I_{P1}$ ). Inset, magnification of the indicated segment of the current trace. In both panels A and B, black bars above the current traces indicate ACh or IVM applications. (C) Kinetics of current decline under long-term application (9.6 sec) of 30  $\mu$ M ACh, in the absence or presence of 0.5  $\mu$ M IVM (performed as described in A and B). In both cases, the application of ACh alone or the co-application of ACh with IVM, the kinetics of current decline was measured from 0.75 sec after the ACh application started until the end of the application. %A stands for the amplitude percentage. Error bars correspond to SEM of N = 10 cells per each condition (ACh alone or ACh + IVM). (D) Normalized ACh response (y-axis) calculated by the current peak ratios that are indicated below the x-axis. Current ratios were extracted from experiments performed as shown in A and B. Black bars correspond to experiments where all applications contained only ACh (e.g., panel A; N = 10). Red bars correspond to experiments where IVM was added during the initial, long-term application of ACh (e.g., panel B; N = 10). Error bars correspond to SEM. Unpaired, two-tailed Student's *t*-tests indicate \*\*\*  $P < 0.0001$ .

IVM with artificial large unilamellar vesicles (LUVs; 6 mM) for 5 minutes, and determining the depletion of IVM from the aqueous solution following a further 20-minutes long ultracentrifugation (50 or 70 percent depletion, depending on the LUVs' lipid composition)<sup>58</sup>. Hence, one may argue that the irreversible inhibition of the chimeric  $\alpha 7$ -GluCl $\beta$ R by IVM is due to the accumulation of IVM in the cell membrane and the consequent increase of the effective concentration of the drug around the receptors. To the best of our knowledge, no data is available regarding the partitioning of ivermectin into the plasma membrane of CHO cells in a period as short as the time of IVM application in the current study (no longer than 10 seconds).

To assess the IVM partitioning into the CHO cell plasma membrane during a short time period, we followed the procedure of Silberberg *et al.*<sup>58</sup> with a few modifications accounting for our experimental conditions. To this end, we incubated 140,000 CHO cells (correspond to 3.2  $\mu$ M plasma membrane lipids<sup>121</sup>) with 4  $\mu$ M IVM for either 0, 15 or 300 seconds, pelleted the cells by a brief centrifugation (30 seconds), and analyzed the extent of IVM removal from the aqueous solution (elaborated in the Supplementary Materials and Methods). Supplementary Fig. S3 shows examples of absorption spectra of supernatant obtained after the CHO cells' sedimentation. These spectra indicate that IVM dissolved in NES containing 0.02% DMSO has an ultraviolet absorption maximum at 245 nm, a wavelength used by others to detect IVM in other solvents<sup>58,122</sup>. The maximum absorbance values were used as a measure for the fraction of IVM removal during the incubation times. Figure 7D indicates that following 5 minutes of incubation, ~24% of IVM was removed from the aqueous solution by the CHO cells. This is less than in artificial LUVs<sup>58</sup>, probably because of the differences in the: membrane lipid composition; IVM hydration conditions; duration of the post-incubation centrifugation; and lipid content (lower in our case as mentioned above). Importantly, within 15 seconds of incubation, no statistically significant amount of IVM was removed from the aqueous solution by the CHO cells (Fig. 7D; e.g. Supplemental Fig. S3). Although these experiments are not sufficiently sensitive to provide the IVM concentration in the CHO cell membrane during the electrophysiological experiments, they indicate that the accumulation of IVM in the membrane is not substantial during the longest IVM applications we employed (10 seconds) (further discussed below).

**Can IVM inhibit homomeric receptors assembled from the *C. elegans* GluCl $\beta$  subunit?** The results presented so far show that IVM strongly inhibits the chimeric  $\alpha 7$ -GluCl $\beta$ R. Since IVM putatively binds in the ion-channel pore domain and this region of the chimeric  $\alpha 7$ -GluCl $\beta$ R is contributed by the *C. elegans* GluCl $\beta$  subunit, an inevitable question emerged: would IVM inhibit homomeric receptors assembled from the *C. elegans* GluCl $\beta$  (GLC-2) subunit? To answer this question, we attempted to express GluCl $\beta$ R homomers in CHO cells, although in a previous study such functional homomers were rarely expressed in CHO cells and provided small responses to 10 mM Glu<sup>79</sup>. Currently, we have used a more powerful transfection reagent (Supplementary Materials and Methods) and challenged the cells with 100 mM Glu. Four of 46 cells gave reliable currents of hundreds of picoamperes at +60 mV (e.g., Fig. 9A and B). These responses were reminiscent of the behavior displayed by homomeric GluCl $\beta$ Rs expressed in *Xenopus* oocytes<sup>4,123</sup>. That is, (i) the responses desensitized (e.g., Fig. 9A) as previously shown under a saturating Glu concentration (see Fig. 7A in Etter *et al.*<sup>123</sup>), and (ii) the responses at +60 mV were larger than the responses obtained at -60 mV, with  $I_{+60\text{mV}}/I_{-60\text{mV}} = 2.8 \pm 0.2$  (mean  $\pm$  SEM) (e.g., Fig. 9A,  $I_{P1}/I_{P0}$ ). Accordingly, the *I/V* curve rectifies outwardly (e.g., Fig. 9B), albeit with less steepness than that observed previously in *Xenopus* oocytes<sup>4</sup>. This difference in the *I/V*-curve steepness is partially because we have used approximately equimolar extra- and intracellular Cl<sup>-</sup> ion concentrations (150.8 mM and 138 mM, respectively), whereas the extracellular and calculated intracellular Cl<sup>-</sup> ion concentrations used in the experiments with *Xenopus* oocytes were 122.6 mM and ~33 mM, respectively<sup>4</sup>. Notably, the responses of the other 42 cells that we patched were very small ( $10.8 \pm 2.6$  pA at +60 mV and  $31.1 \pm 5.6$  pA at -60 mV), providing  $I_{+60\text{mV}}/I_{-60\text{mV}} = 0.26 \pm 0.06$ ; and therefore these responses were considered as nonspecific and irrelevant to the homomeric GluCl $\beta$ R.

Figure 9A and C, also shows that pre-application of 2  $\mu$ M IVM for 10 seconds leads to the inhibition of ~67% of the response of the homomeric GluCl $\beta$ Rs to 100 mM Glu ( $I_{P2}/I_{P1}$ ). Further application of 100 mM Glu after a wash of 25 seconds provided peak  $I_{P3}$ , which revealed that most of the initial response disappeared (Fig. 9A and C,  $I_{P3}/I_{P1}$ ). Note that, in spite of the efficient perfusion system, which provides a time constant of activation at the millisecond range ( $33.1 \pm 3.7$  ms), the Glu-elicited currents slowly returned to baseline upon the application of wash. This slow current decline is probably due to the very high concentration of the applied Glu (100 mM), which is ~260 times the EC<sub>50</sub> determined in *Xenopus* oocytes (380  $\mu$ M) for the homomeric GluCl $\beta$ R<sup>4</sup>.

## Discussion

Cys-loop receptor chimeras have long been used to shed light on the interplay between the ligand-binding domain and the ion-channel pore domain<sup>55,80,81,97,98,124–129</sup>. Here we used a highly expressible, homomeric  $\alpha 7$ -GluCl $\beta$  chimeric receptor in an attempt to understand why IVM does not activate the *C. elegans* homomeric GluCl $\beta$ R although it can activate the *C. elegans* heteromeric GluCl $\alpha/\beta$ R. The rationale behind our decision to work with a chimera having the extracellular domain of the  $\alpha 7$ -nAChR was based on the assumption that the LigBD-pore domain interface might affect IVM action. This assumption emerged because of the following reasons. (i) IVM strongly potentiates ACh-elicited currents in the  $\alpha 7$ -nAChR<sup>54</sup>. (ii) In the GluCl $\alpha_{\text{cryst}}$ R, the disaccharide and lactone moieties of IVM form van der Waals interactions with the M2-M3 loop<sup>77</sup> that is located at the LigBD-pore domain interface. (iii) The M2-M3 loop of Cys-loop receptors interacts with the  $\beta 1\beta 2$ , Cys and  $\beta 8\beta 9$  loops of the ligBD as well as with the pre-M1 segment to couple agonist binding to channel gating<sup>50,83–98,130–136</sup>. (iv) Incorporation of the GluCl $\beta$  subunit in GluClR assemblies increases the sensitivity of the receptor to IVM<sup>78</sup>, which suggests that IVM interacts with the GluCl $\beta$  subunit. We therefore expected that IVM would, at least, potentiate the response of the chimeric  $\alpha 7$ -GluCl $\beta$ R to ACh. To our great surprise, IVM was found here to strongly inhibit the chimeric  $\alpha 7$ -GluCl $\beta$ R.

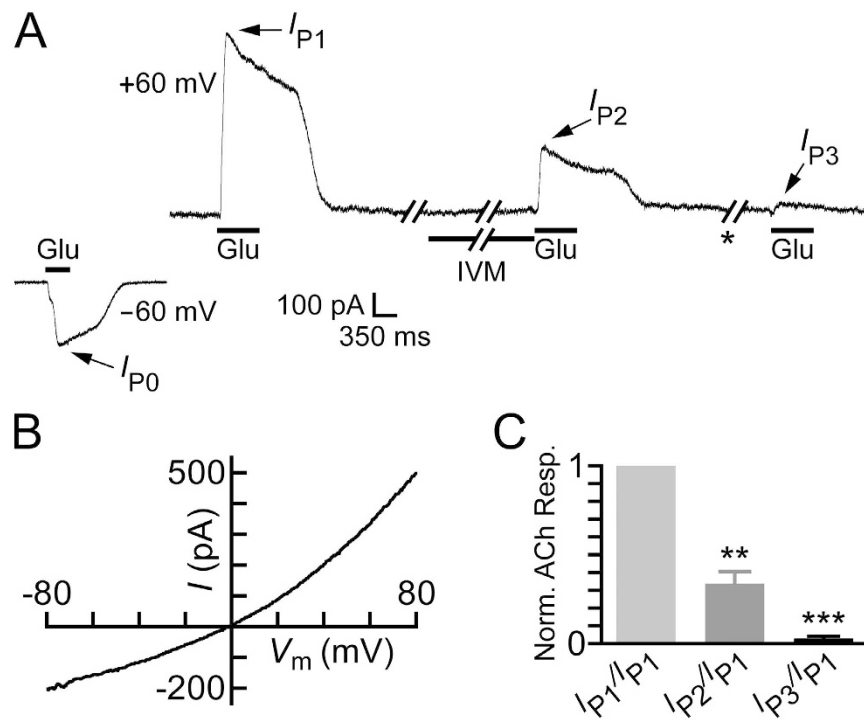


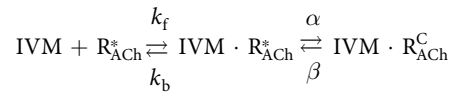
**Figure 9. Effect of IVM on homomeric GluCl $\beta$  receptors.** (A) Representative current traces obtained by the indicated application protocol. Glu (100 mM) was applied for either 350 ms to obtain peak  $I_{P0}$  at  $-60$  mV, or 600 ms to obtain peaks  $I_{P1}$ ,  $I_{P2}$  and  $I_{P3}$  at  $+60$  mV. Note that the responses at both membrane voltages,  $-60$  and  $+60$  mV, start to desensitize appreciably before the end of Glu application. IVM ( $2\mu\text{M}$ ) was applied for 10 seconds. Asterisk indicates a 25-sec-long wash between the second and third Glu applications. (B) Current-voltage ( $I/V$ ) relations obtained in a different cell than in A upon the application of Glu (100 mM) over a voltage ramp lasting 200 ms. (C) Normalized ACh response (y-axis) calculated by the current peak ratios that are indicated below the x-axis. Current ratios were extracted from experiments performed as shown in (A). Mean  $\pm$  SEM of four cells are presented. Paired, two-tailed Student's  $t$ -tests indicate that  $**0.001 < P < 0.01$  and  $***P < 0.0002$ .

Interestingly, IVM negatively modulates a few other Cys-loop receptors<sup>55,137,138</sup>. Yet, little is known about the mechanism of the IVM inhibitory phenomenon. Here, based on experiments where IVM was applied prior to ACh, we suggest that IVM can bind to the resting (closed) state of the  $\alpha 7$ -GluCl $\beta$ R and stabilize this conformation for a long duration. However, we do not exclude the possibility that the stabilized conformation corresponds to a desensitized-like state, since unliganded as well as liganded Cys-loop receptors can interconvert from the resting state to a desensitized state directly without opening; for instance, the neuronal  $\alpha 4\beta 2$  nAChR<sup>115</sup>.

IVM binds in the periphery of the ion-channel pore domain of the GluCl $\alpha_{\text{cryst}}$ <sup>R77</sup>, and it was likewise suggested to bind in a homologous peripheral site in the GlyR<sup>137</sup>. Assuming that IVM also binds in the periphery of the ion-channel pore domain of the chimeric  $\alpha 7$ -GluCl $\beta$ R, then the possibility of competitive inhibition by IVM is excluded. Uncompetitive inhibition, which requires receptor-activator complex formation prior to binding of the inhibitor<sup>139</sup>, is also excluded because IVM can bind already before ACh association with the  $\alpha 7$ -GluCl $\beta$ R (e.g., Fig. 4). Since non-competitive inhibition can occur with or without the presence of the activator, IVM most likely acts as a non-competitive inhibitor of the chimeric  $\alpha 7$ -GluCl $\beta$ R (e.g., Figs 4 and 5). Therefore, the  $\text{IC}_{50}$  determined in Fig. 3 (156 nM) actually corresponds to the inhibition constant ( $K_i$ )<sup>139</sup>.

The response of the chimeric  $\alpha 7$ -GluCl $\beta$ R to ACh declines slowly after reaching to its peak. This decline could be attributed, at least in part, to a loss of electrochemical driving force for  $\text{Cl}^-$  ions, as discussed in the "Results". However, one cannot exclude the possibility that a fraction of this decline corresponds to channels' closing in the presence of the agonist due to desensitization. When IVM was added to an already activated receptor population, immediately after the response reached to its peak, the decline of the current became faster and the extent of current loss at the end of the co-application period was larger. As discussed in detail in the "Results" (Fig. 6), the faster and stronger decline in the  $\text{Cl}^-$  conductance and the lesser decrease in  $[\text{Cl}]_i$  and  $V_{\text{DF}}$  during the co-application of ACh with IVM, as compared with the application of ACh alone, strongly suggest that, in the presence of IVM, the receptor adopts a conformation that hinders chloride ion flow. The exponential fits to the specific IVM-dependent  $\text{Cl}^-$ -conductance ( $G_{\text{IVM}}$ ) decay (Fig. 6) allowed us to obtain the affinity of the  $\alpha 7$ -GluCl $\beta$ R for IVM when the drug is applied after activation ( $K_d = 1.4\mu\text{M}$ ; Fig. 6N). When IVM is applied prior to the activation by ACh, the affinity of the receptor for IVM is nine times higher ( $K_i = 156$  nM; Fig. 3). Hence, we suggest that IVM can bind to two distinct receptor states. One state is possibly the resting state and the other state is likely to be an open state of the  $\alpha 7$ -GluCl $\beta$ R. We further suggest that IVM binding to the open state induces a

conformational change that results in pore closure. In respect to IVM association with the open state, the aforementioned kinetic model should therefore be revised as follows.



where  $k_f$  and  $k_b$  are the rate constants described above in the first kinetic model, and  $\alpha$  and  $\beta$  are the rates of receptor interconversion between the IVM-bound open state ( $\text{IVM} \cdot \text{R}_{\text{ACh}}^*$ ) and the IVM-bound non-conducting (closed) state ( $\text{IVM} \cdot \text{R}_{\text{ACh}}^{\text{C}}$ ). We could not determine the receptor interconversion rates, but it is reasonable to assume that if  $\alpha \gg \beta$ , then the IVM-bound closed conformation would be stable for a long duration.

Most recently, the three dimensional structure of a homomeric  $\alpha 1$  GlyR from the zebrafish (termed GlyR<sub>EM</sub>) was elucidated by electron cryo-microscopy (ECM) in conformations that correspond to the receptor complexed with either glycine alone or with both glycine and IVM<sup>140</sup>. These ECM structures indicate that the ion-channel pore of a receptor occupied by both glycine and IVM is narrower than that of a receptor occupied by glycine alone. Yet, the most constricted portion of the doubly occupied (glycine/IVM) GlyR<sub>EM</sub> has a diameter of 5 Å, which is sufficiently wide to allow Cl<sup>-</sup> ions to pass<sup>140</sup>. We speculate that the association of IVM with ACh-occupied open  $\alpha 7$ -GluCl $\beta$ R leads to constriction of the ion-channel pore, but unlike the case of the doubly occupied GlyR<sub>EM</sub>, here the constriction of the  $\alpha 7$ -GluCl $\beta$ R is not sufficiently wide to allow Cl<sup>-</sup> ions to flow across the ion-channel pore.

The capability of ACh-elicited currents to recover after the first response to long-term application of ACh alone (Fig. 7A and C, black bars), clearly indicates that no change in the size of the receptor population has occurred. This conclusion excludes the possibility that functional rundown accompanied with permanent inactivation took place. Hence, the gradual recovery seen in Fig. 7A could indicate that reversible desensitization or/and a decrease in  $V_{\text{DF}}$  underlie the lack of current when ACh is reapplied alone 5 to 70 seconds after the end of the initial long-term ACh application (see also Fig. 7C, black bars). We therefore conclude that the small responses to ACh that were obtained after the co-application of ACh with IVM (Fig. 7B and C, red bars) likely correspond to a receptor population that is 'stuck' in the above-mentioned channel-constricted conformation.

When IVM is added after the ACh-elicited current reached to its peak, it most likely associates with open receptors. The calculation of the time constant of  $G_{\text{IVM}}$  decay (Fig. 6N) allowed us to determine the residency time of IVM bound to the  $\alpha 7$ -GluCl $\beta$ R ( $1/k_b = \sim 2.5$  sec). This value means that a few seconds after removal of water-soluble IVM from around the cell by a wash, the inhibitory effect should have been weakened due to IVM dissociation and lateral diffusion in the membrane. However, the responses were not even partially recovered after the first exposure of ACh-bound open  $\alpha 7$ -GluCl $\beta$ R to IVM (Figs 7 and 8), indicating that there might be an additional binding step that possibly causes trapping of IVM in the pore periphery. Yet, one cannot exclude with absolute certainty the possibility that the irreversibility of the inhibition could be due to a steady, high membranous IVM concentration encountered by the receptors, rather than an irreversible trapping of IVM by the receptors. This possibility arises because, within time, IVM tends to accumulate in lipid bilayers due to its lipophilic properties, and it cannot be removed from the lipidic phase under physiological conditions. Previous studies involving IVM accumulation in artificial lipid bilayers or biological membranes<sup>58,120</sup> are relevant to relatively much longer incubation times than used in the current study (detailed in the "Results"). Indeed, we found that no substantial accumulation of IVM in the membrane of CHO cells is apparent during a 15-sec-long incubation with each other (Fig. 7D and Supplementary Fig. S3). The longest time of exposure to IVM in the electrophysiological experiments performed here was 10 seconds. The perfusion exchange in our system removes soluble small molecules from around the cell within less than a second, as can be judged by the time of the current's return to the baseline when replacing ACh-containing solution by a wash ( $407 \pm 34$  ms, in the experiments represented by Figs 7A and 8A). This means that, after 10 seconds of IVM application, it probably takes less than 1 second to remove all the water-soluble IVM molecules from around the cell, as well. At this time point, no further IVM is available for binding by the receptors, except for those membrane-embedded IVM molecules that, as said above, do not likely reflect a substantial accumulation.

Noteworthy, the effect of IVM might take place due to IVM partitioning into the membrane at the site of its action, or by IVM molecules that partition into the membrane far from their targets and approach their binding sites by lateral movement within the lipid bilayer. Lateral movement of a fluorescently labeled IVM probe in biological membranes was previously determined to be slow, with a lateral diffusion coefficient ( $D_L$ ) of  $14 \cdot 10^{-10}$  cm<sup>2</sup>/s (see page 554 in Martin and Kusel<sup>120</sup>, under "The lateral mobility of the ivermectin probe"). In the six experiments represented by Fig. 5A (e.g., red trace), the time between the start of ACh or IVM applications and the onset of their effects was  $67 \pm 7$  or  $132 \pm 24$  milliseconds, respectively. Taking into account the differences in accessibility and complexity between the ACh and IVM binding sites, the two-fold slower onset of effect observed for IVM is reasonable if IVM acts at the site of its partitioning. In this context, it is intriguing to point out that in the GluCl $\alpha_{\text{cryst}}$  receptor the disaccharide and lactone moieties of IVM interact with the M2-M3 loop<sup>77</sup> that is putatively situated above the lipid leaflet in all Cys-loop receptors. So, partitioning of IVM into the membrane at the site of action perhaps involves a recognition step that occurs outside of the membrane (still have to be studied).

Collectively, our IVM partitioning experiments and the arguments raised above suggest that the concentration of IVM in the perfused solution approximates the concentration of IVM in the membrane at the end of the 10-sec-long IVM application. Hence, our calculation of  $k_b$  based on the concentration of IVM in the perfused solution is a reasonable approximation. Still, one may argue that since the washes do not extract IVM from the membrane, the irreversibility may reflect an exchange between receptor-bound and membrane-resident IVM molecules. The counter argument is based on Fig. 6K, which indicates that 740 milliseconds after the application of 0.5  $\mu$ M IVM, there is already a statistically significant IVM-dependent decrease in the chloride conductance by  $20 \pm 2\%$  ( $P = 0.0005$ , paired, two-tailed Student's  $t$ -test). This IVM concentration (0.5  $\mu$ M) does not exert the

maximal inhibitory effect according to the declining rate of the chloride conductance (Fig. 6). Yet, we did not observe even a partial recovery of the initial response following IVM removal from the external solution and the subsequent ACh applications (Figs 7B and 8B); which likely indicates that IVM is trapped in its binding site(s) for a long duration.

In conclusion, the results presented here suggest that IVM can bind to both, the resting and active states of the  $\alpha 7$ -GluCl $\beta$ R. After initial binding of the drug to the active (open) state, it accelerates pore constriction to a degree that impedes Cl<sup>-</sup> ion flow through the ion-channel pore. We suggest that at the time the pore becomes constricted in a non-conductive conformation, IVM is likely trapped between the transmembrane segments for a long duration and it reciprocally locks the pore-lining segments. As such, gating motions necessary for re-opening of the ion-channel pore are prevented.

So far, it was not known why homomeric receptors assembled from the *C. elegans* GluCl $\beta$  (GLC-2) subunit could not be activated by IVM<sup>4,7,8,76</sup>. The current study provides an answer to this question by demonstrating that IVM actually inhibits the responses of the *C. elegans* homomeric GluCl $\beta$ R to Glu (Fig. 9). IVM likely binds in the periphery of the ion-channel pore domain, between adjacent subunits of the homomeric GluCl $\beta$ R, akin to the case of the GluCl $\alpha_{\text{cryst}}$ R. If so, IVM is accommodated by the homomeric GluCl $\beta$ R at  $\beta/\beta$  intersubunit interfaces. In a previous study, we inferred that the subunits of the *C. elegans* heteromeric GluCl $\alpha$ (GLC-1)/ $\beta$ (GLC-2) receptor are arranged in an anticlockwise  $\beta$ - $\alpha$ - $\beta$ - $\alpha$ - $\alpha$  fashion, as viewed from the extracellular milieu<sup>79</sup>. This subunit arrangement does not have  $\beta/\beta$  intersubunit interfaces. Hence, we further hypothesize that in the IVM-activatable heteromeric GluCl $\alpha/\beta$ R, the subunit arrangement precludes potential restraints that could have emerged by IVM binding at such  $\beta/\beta$  interfaces.

## Materials and Methods

“Homology modelling”, “DNA construct and preparation of cells for electrophysiological experiments” and “Whole-cell patch clamp recordings” are described in the Supplementary Materials and Methods.

**Data analysis.** Analyses were performed using the Clampfit 10 program implemented in pClamp 10, and the GraphPad Prism software.

Dose-response curves were fitted to the data points by a nonlinear regression using the Hill equation 1,

$$\frac{I}{I_{\max}} = \frac{1}{1 + 10^{(\log EC_{50} - \log [ACh])n_H}} \quad (1)$$

where  $I$  is the current response,  $I_{\max}$  is the maximal current response,  $EC_{50}$  is the agonist effective concentration that elicits 50% of maximal current response,  $[ACh]$  is the concentration of acetylcholine, and  $n_H$  is the Hill coefficient.

In the case of inhibition of the current response, curves were fitted to the data points by a nonlinear regression using the Hill equation 2,

$$\frac{I}{I_{\max}} = 1 - \frac{1}{1 + 10^{(\log IC_{50} - \log [IVM])n_H}} \quad (2)$$

where  $I$  is the current response,  $I_{\max}$  is the maximal current response,  $IC_{50}$  is the IVM concentration that inhibits 50% of the current response,  $[IVM]$  is the concentration of ivermectin, and  $n_H$  is the Hill coefficient.

The declining phase of the currents was fitted with an exponential time course to give the time constant of current decline by using equation 3,

$$I = [(I_p - I_s)^{-t/\tau}] + I_s \quad (3)$$

or its bi-exponential variant where appropriate, using data that relates to ~90% of the period between the peak of the current and the termination of a typical 5.5- or 9.6-sec-long ACh (or ACh + IVM) application (i.e., the fitting was performed from the point of IVM addition).  $I$  is the current,  $I_p$  is the peak of the current,  $I_s$  is the steady state current,  $t$  is the time, and  $\tau$  is the time constant of current decline.

To calculate the changes in the intracellular concentration of Cl<sup>-</sup> ions ( $[Cl]_i$ ) in the voltage-ramp experiments, the Nernst equation (4) was used as follows:

$$E_{Cl} = E_{\text{rev}} = \frac{RT}{zF} \ln \frac{[Cl]_o}{[Cl]_i} \quad (4)$$

where  $E_{Cl}$  is the Nernst (equilibrium) potential for Cl<sup>-</sup> ions;  $E_{\text{rev}}$  is the measured reversal potential;  $R$  and  $F$  are the gas and Faraday constants, respectively;  $T$  is the absolute temperature (298.15 K);  $z$  is the valance of a Cl<sup>-</sup> ion (-1);  $[Cl]_o$  is the extracellular concentration of Cl<sup>-</sup> ions; and  $[Cl]_i$  is the intracellular concentration of Cl<sup>-</sup> ions.

Chord conductance ( $G$ ) was calculated by using equation 5 as follows:

$$G = I/(V_m - E_{\text{rev}}) \quad (5)$$

where  $G$  is the chloride conductance,  $I$  corresponds to the current measured at the respective membrane voltage ( $V_m$ ), and  $E_{\text{rev}}$  is the reversal potential.

The relationship between the conductance values and time was plotted for each cell, and the time constant of conductance decay was determined by fitting an exponential curve to the data points using equation 6 as follows:

$$G_{Cl}(t) = \{G_{Cl}(max) - G_{Cl}(plat)\}(e^{-t/\tau}) + G_{Cl}(plat) \quad (6)$$

or its bi-exponential variant where appropriate.  $G_{Cl}(t)$  is the chloride conductance at a given time;  $G_{Cl}(max)$  and  $G_{Cl}(plat)$  are the chloride conductance values at the maximum and the plateau, respectively;  $t$  is the time; and  $\tau$  is the time constant of the chloride-conductance decay to the plateau.

To calculate the IVM association ( $k_f$ ) and dissociation ( $k_b$ ) rate constants, a curve was fitted to the  $1/\tau_{IVM}$  values by a linear regression using equation 7 as follows:

$$1/\tau_{IVM} = k_f[IVM] + k_b \quad (7)$$

where  $\tau_{IVM}$  is the time constant of the IVM-dependent  $Cl^-$ -conductance decay, and  $[IVM]$  is the concentration of IVM.

## References

- Crump, A. & Omura, S. Ivermectin, 'wonder drug' from Japan: the human use perspective. *Proc Jpn Acad Ser B Phys Biol Sci* **87**, 13–28 (2011).
- Campbell, W. C. History of avermectin and ivermectin, with notes on the history of other macrocyclic lactone antiparasitic agents. *Curr Pharm Biotechnol* **13**, 853–865 (2012).
- Geary, T. G. Ivermectin 20 years on: maturation of a wonder drug. *Trends Parasitol* **21**, 530–532 (2005).
- Cully, D. F. *et al.* Cloning of an avermectin-sensitive glutamate-gated chloride channel from *Caenorhabditis elegans*. *Nature* **371**, 707–711 (1994).
- Etter, A., Cully, D. F., Schaeffer, J. M., Liu, K. K. & Arena, J. P. An amino acid substitution in the pore region of a glutamate-gated chloride channel enables the coupling of ligand binding to channel gating. *J Biol Chem* **271**, 16035–16039 (1996).
- Dent, J. A., Davis, M. W. & Avery, L. *avr-15* encodes a chloride channel subunit that mediates inhibitory glutamatergic neurotransmission and ivermectin sensitivity in *Caenorhabditis elegans*. *EMBO J* **16**, 5867–5879 (1997).
- Vassilatis, D. K. *et al.* Genetic and biochemical evidence for a novel avermectin-sensitive chloride channel in *Caenorhabditis elegans*. Isolation and characterization. *J Biol Chem* **272**, 33167–33174 (1997).
- Li, P., Slimko, E. M. & Lester, H. A. Selective elimination of glutamate activation and introduction of fluorescent proteins into a *Caenorhabditis elegans* chloride channel. *FEBS Lett* **528**, 77–82 (2002).
- Slimko, E. M., McKinney, S., Anderson, D. J., Davidson, N. & Lester, H. A. Selective electrical silencing of mammalian neurons *in vitro* by the use of invertebrate ligand-gated chloride channels. *J Neurosci* **22**, 7373–7379 (2002).
- Cook, A. *et al.* *Caenorhabditis elegans* ivermectin receptors regulate locomotor behaviour and are functional orthologues of *Haemonchus contortus* receptors. *Mol Biochem Parasitol* **147**, 118–125 (2006).
- Geary, T. G. *et al.* *Haemonchus contortus*: ivermectin-induced paralysis of the pharynx. *Exp Parasitol* **77**, 88–96 (1993).
- Brownlee, D. J., Holden-Dye, L. & Walker, R. J. Actions of the anthelmintic ivermectin on the pharyngeal muscle of the parasitic nematode, *Ascaris suum*. *Parasitology* **115** (Pt 5), 553–561 (1997).
- Dent, J. A., Smith, M. M., Vassilatis, D. K. & Avery, L. The genetics of ivermectin resistance in *Caenorhabditis elegans*. *Proc Natl Acad Sci USA* **97**, 2674–2679 (2000).
- Moreno, Y., Nabhan, J. F., Solomon, J., Mackenzie, C. D. & Geary, T. G. Ivermectin disrupts the function of the excretory-secretory apparatus in microfilariae of *Brugia malayi*. *Proc Natl Acad Sci USA* **107**, 20120–20125 (2010).
- Geary, T. G. & Moreno, Y. Macrocyclic lactone anthelmintics: spectrum of activity and mechanism of action. *Curr Pharm Biotechnol* **13**, 866–872 (2012).
- Wolstenholme, A. J., Maclean, M. J., Coates, R., McCoy, C. J. & Reaves, B. J. How do the macrocyclic lactones kill filarial nematode larvae? *Invert Neurosci* **16**, 7 (2016).
- Wolstenholme, A. J. Glutamate-gated chloride channels. *J Biol Chem* **287**, 40232–40238 (2012).
- Karlin, A. Emerging structure of the nicotinic acetylcholine receptors. *Nat Rev Neurosci* **3**, 102–114 (2002).
- Lester, H. A., Dibas, M. I., Dahan, D. S., Leite, J. F. & Dougherty, D. A. Cys-loop receptors: new twists and turns. *Trends Neurosci* **27**, 329–336 (2004).
- Taylor, P. *et al.* Structure-guided drug design: conferring selectivity among neuronal nicotinic receptor and acetylcholine-binding protein subtypes. *Biochem Pharmacol* **74**, 1164–1171 (2007).
- Taly, A., Corringer, P. J., Guedin, D., Lestage, P. & Changeux, J. P. Nicotinic receptors: allosteric transitions and therapeutic targets in the nervous system. *Nat Rev Drug Discov* **8**, 733–750 (2009).
- Boulin, T. *et al.* Positive modulation of a Cys-loop acetylcholine receptor by an auxiliary transmembrane subunit. *Nat Neurosci* **15**, 1374–1381 (2012).
- Sine, S. M. End-plate acetylcholine receptor: structure, mechanism, pharmacology, and disease. *Physiol Rev* **92**, 1189–1234 (2012).
- Dineley, K. T., Pandya, A. A. & Yakel, J. L. Nicotinic ACh receptors as therapeutic targets in CNS disorders. *Trends Pharmacol Sci* **36**, 96–108 (2015).
- Chatzidakis, A. & Millar, N. S. Allosteric modulation of nicotinic acetylcholine receptors. *Biochem Pharmacol* **97**, 408–417 (2015).
- Stokes, C., Treinin, M. & Papke, R. L. Looking below the surface of nicotinic acetylcholine receptors. *Trends Pharmacol Sci* **36**, 514–523 (2015).
- Corradi, J. & Bouzat, C. Understanding the Bases of Function and Modulation of  $\alpha 7$  Nicotinic Receptors: Implications for Drug Discovery. *Mol Pharmacol* **90**, 288–299 (2016).
- Lummis, S. C. 5-HT(3) receptors. *J Biol Chem* **287**, 40239–40245 (2012).
- Kesters, D. *et al.* Structural basis of ligand recognition in 5-HT3 receptors. *EMBO Rep* **14**, 49–56 (2013).
- Zheleznova, N. N., Sedelnikova, A. & Weiss, D. S. Function and modulation of  $\delta$ -containing GABAA receptors. *Psychoneuroendocrinology* **34**, S67–S73 (2009).
- Akk, G. & Steinbach, J. H. Structural studies of the actions of anesthetic drugs on the gamma-aminobutyric acid type A receptor. *Anesthesiology* **115**, 1338–1348 (2011).
- Liang, J. & Olsen, R. W. Alcohol use disorders and current pharmacological therapies: the role of GABA(A) receptors. *Acta Pharmacol Sin* **35**, 981–993 (2014).
- Seljeset, S., Laverty, D. & Smart, T. G. Inhibitory neurosteroids and the GABAA receptor. *Adv Pharmacol* **72**, 165–187 (2015).
- Breitinger, H. G. & Becker, C. M. The inhibitory glycine receptor-simple views of a complicated channel. *ChemBiochem* **3**, 1042–1052 (2002).
- Colquhoun, D. & Sivilotti, L. G. Function and structure in glycine receptors and some of their relatives. *Trends Neurosci* **27**, 337–344 (2004).
- Betz, H. & Laube, B. Glycine receptors: recent insights into their structural organization and functional diversity. *J Neurochem* **97**, 1600–1610 (2006).
- Harvey, R. J., Topf, M., Harvey, K. & Rees, M. I. The genetics of hyperekplexia: more than startle! *Trends Genet* **24**, 439–447 (2008).

38. Sivilotti, L. G. What single-channel analysis tells us of the activation mechanism of ligand-gated channels: the case of the glycine receptor. *J Physiol* **588**, 45–58 (2010).
39. Lynch, T. & Lynch, J. W. Molecular mechanisms of Cys-loop ion channel receptor modulation by ivermectin. *Front Mol Neurosci* **5**, 60 (2012).
40. Schaefer, N., Langlhofer, G., Kluck, C. J. & Villmann, C. Glycine receptor mouse mutants: model systems for human hyperekplexia. *Br J Pharmacol* **170**, 933–952 (2013).
41. Hardie, R. C. A histamine-activated chloride channel involved in neurotransmission at a photoreceptor synapse. *Nature* **339**, 704–706 (1989).
42. Gisselmann, G., Pusch, H., Hovemann, B. T. & Hatt, H. Two cDNAs coding for histamine-gated ion channels in *D. melanogaster*. *Nat Neurosci* **5**, 11–12 (2002).
43. Zheng, Y. *et al.* Identification of two novel *Drosophila melanogaster* histamine-gated chloride channel subunits expressed in the eye. *J. Biol. Chem.* **277**, 2000–2005 (2002).
44. Williams, M. & Risley, E. A. Interaction of avermectins with [3H]beta-carboline-3-carboxylate ethyl ester and [3H]diazepam binding sites in rat brain cortical membranes. *Eur J Pharmacol* **77**, 307–312 (1982).
45. Olsen, R. W. & Snowman, A. M. Avermectin B1a modulation of gamma-aminobutyric acid/benzodiazepine receptor binding in mammalian brain. *J Neurochem* **44**, 1074–1082 (1985).
46. Sigel, E. & Baur, R. Effect of avermectin B1a on chick neuronal gamma-aminobutyrate receptor channels expressed in *Xenopus* oocytes. *Mol Pharmacol* **32**, 749–752 (1987).
47. Krusek, J. & Zemkova, H. Effect of ivermectin on gamma-aminobutyric acid-induced chloride currents in mouse hippocampal embryonic neurones. *Eur J Pharmacol* **259**, 121–128 (1994).
48. Adelsberger, H., Lepier, A. & Dudel, J. Activation of rat recombinant alpha(1)beta(2)gamma(2S) GABA(A) receptor by the insecticide ivermectin. *Eur J Pharmacol* **394**, 163–170 (2000).
49. Shan, Q., Haddrill, J. L. & Lynch, J. W. Ivermectin, an unconventional agonist of the glycine receptor chloride channel. *J Biol Chem* **276**, 12556–12564 (2001).
50. Pless, S. A. & Lynch, J. W. Magnitude of a conformational change in the glycine receptor beta1-beta2 loop is correlated with agonist efficacy. *J Biol Chem* **284**, 27370–27376 (2009).
51. Lynch, T. & Lynch, J. W. Ivermectin binding sites in human and invertebrate Cys-loop receptors. *Trends Pharmacol Sci* (2012).
52. Menez, C., Sutra, J. F., Prichard, R. & Lespine, A. Relative neurotoxicity of ivermectin and moxidectin in *Mdr1ab (-/-)* mice and effects on mammalian GABA(A) channel activity. *PLoS Negl Trop Dis* **6**, e1883 (2012).
53. Wang, Q. & Lynch, J. W. A comparison of glycine- and ivermectin-mediated conformational changes in the glycine receptor ligand-binding domain. *Int J Biochem Cell Biol* **44**, 335–340 (2012).
54. Krause, R. M. *et al.* Ivermectin: a positive allosteric effector of the alpha7 neuronal nicotinic acetylcholine receptor. *Mol Pharmacol* **53**, 283–294 (1998).
55. Collins, T. & Millar, N. S. Nicotinic acetylcholine receptor transmembrane mutations convert ivermectin from a positive to a negative allosteric modulator. *Mol Pharmacol* **78**, 198–204 (2010).
56. Khakh, B. S., Proctor, W. R., Dunwiddie, T. V., Labarca, C. & Lester, H. A. Allosteric control of gating and kinetics at P2X(4) receptor channels. *J Neurosci* **19**, 7289–7299 (1999).
57. Priel, A. & Silberberg, S. D. Mechanism of ivermectin facilitation of human P2X4 receptor channels. *J Gen Physiol* **123**, 281–293 (2004).
58. Silberberg, S. D., Li, M. & Swartz, K. J. Ivermectin Interaction with transmembrane helices reveals widespread rearrangements during opening of P2X receptor channels. *Neuron* **54**, 263–274 (2007).
59. Habermacher, C., Dunning, K., Chataigneau, T. & Grutter, T. Molecular structure and function of P2X receptors. *Neuropharmacology* **104**, 18–30 (2016).
60. Yates, D. M., Portillo, V. & Wolstenholme, A. J. The avermectin receptors of *Haemonchus contortus* and *Caenorhabditis elegans*. *Int J Parasitol* **33**, 1183–1193 (2003).
61. Lynch, T. *et al.* Molecular basis for convergent evolution of glutamate recognition by pentameric ligand-gated ion channels. *Sci Rep* **5**, 8558 (2015).
62. Delany, N. S., Laughton, D. L. & Wolstenholme, A. J. Cloning and localisation of an avermectin receptor-related subunit from *Haemonchus contortus*. *Mol Biochem Parasitol* **97**, 177–187 (1998).
63. Jagannathan, S. *et al.* Ligand-gated chloride channel subunits encoded by the *Haemonchus contortus* and *Ascaris suum* orthologues of the *Caenorhabditis elegans* gbr-2 (avr-14) gene. *Mol Biochem Parasitol* **103**, 129–140 (1999).
64. Dufour, V., Beech, R. N., Wever, C., Dent, J. A. & Geary, T. G. Molecular cloning and characterization of novel glutamate-gated chloride channel subunits from *Schistosoma mansoni*. *PLoS Pathog* **9**, e1003586 (2013).
65. Lynch, T., Cromer, B. A., Dufour, V. & Laube, B. Comparative pharmacology of flatworm and roundworm glutamate-gated chloride channels: Implications for potential anthelmintics. *Int J Parasitol Drugs Drug Resist* **4**, 244–255 (2014).
66. Eguchi, Y. *et al.* Functional characterization of *Musca* glutamate- and GABA-gated chloride channels expressed independently and coexpressed in *Xenopus* oocytes. *Insect Mol Biol* **15**, 773–783 (2006).
67. Dong, Y., Chen, Y., Wei, Q., Su, J. & Gao, C. Cloning and Polymorphism Analysis of Glutamate-Gated Chloride Channel Gene of *Laodelphax striatellus* (Hemiptera: Delphacidae). *Florida Entomologist* **96**, 1168–1174 (2013).
68. Furutani, S. *et al.* Exon 3 splicing and mutagenesis identify residues influencing cell surface density of heterologously expressed silkworm (*Bombyx mori*) glutamate-gated chloride channels. *Mol Pharmacol* **86**, 686–695 (2014).
69. Kita, T., Ozoe, F. & Ozoe, Y. Expression pattern and function of alternative splice variants of glutamate-gated chloride channel in the housefly *Musca domestica*. *Insect Biochem Mol Biol* **45**, 1–10 (2014).
70. Meyers, J. I. *et al.* Characterization of the target of ivermectin, the glutamate-gated chloride channel, from *Anopheles gambiae*. *J Exp Biol* **218**, 1478–1486 (2015).
71. Wu, S. F. *et al.* Expression pattern and pharmacological characterisation of two novel alternative splice variants of the glutamate-gated chloride channel in the small brown planthopper *Laodelphax striatellus*. *Pest Manag Sci* (2016).
72. Cornejo, I. *et al.* Identification and functional expression of a glutamate- and avermectin-gated chloride channel from *Caligus rogercresceyi*, a southern Hemisphere sea louse affecting farmed fish. *PLoS Pathog* **10**, e1004402 (2014).
73. Kehoe, J. *et al.* *Aplysia* cys-loop glutamate-gated chloride channels reveal convergent evolution of ligand specificity. *J Mol Evol* **69**, 125–141 (2009).
74. Cully, D. F., Pareess, P. S., Liu, K. K., Schaeffer, J. M. & Arena, J. P. Identification of a *Drosophila melanogaster* glutamate-gated chloride channel sensitive to the antiparasitic agent ivermectin. *J Biol Chem* **271**, 20187–20191 (1996).
75. McCavera, S., Rogers, A. T., Yates, D. M., Woods, D. J. & Wolstenholme, A. J. An ivermectin-sensitive glutamate-gated chloride channel from the parasitic nematode *Haemonchus contortus*. *Mol Pharmacol* **75**, 1347–1355 (2009).
76. Daeffler, K. N., Lester, H. A. & Dougherty, D. A. Functional Evaluation of Key Interactions Evident in the Structure of the Eukaryotic Cys-Loop Receptor GluCl. *ACS Chem Biol* (2014).
77. Hibbs, R. E. & Gouaux, E. Principles of activation and permeation in an anion-selective Cys-loop receptor. *Nature* **474**, 54–60 (2011).
78. Frazier, S. J., Cohen, B. N. & Lester, H. A. An engineered glutamate-gated chloride (GluCl) channel for sensitive, consistent neuronal silencing by ivermectin. *J Biol Chem* **288**, 21029–21042 (2013).



79. Degani-Katzav, N., Gortler, R., Gorodetzki, L. & Paas, Y. Subunit stoichiometry and arrangement in a heteromeric glutamate-gated chloride channel. *Proc Natl Acad Sci USA* **113**, E644–653 (2016).
80. Sunesen, M. *et al.* Mechanism of Cl<sup>-</sup> selection by a glutamate-gated chloride (GluCl) receptor revealed through mutations in the selectivity filter. *J Biol Chem* **281**, 14875–14881 (2006).
81. Bar-Lev, D. D., Degani-Katzav, N., Perelman, A. & Paas, Y. Molecular dissection of Cl<sup>-</sup>-selective Cys-loop receptor points to components that are dispensable or essential for channel activity. *J Biol Chem* **286**, 43830–43841 (2011).
82. Forrester, S. G., Prichard, R. K., Dent, J. A. & Beech, R. N. Haemonchus contortus: HcGluCl<sub>a</sub> expressed in *Xenopus* oocytes forms a glutamate-gated ion channel that is activated by ibotenate and the antiparasitic drug ivermectin. *Mol Biochem Parasitol* **129**, 115–121 (2003).
83. Boileau, A. J. & Czajkowski, C. Identification of transduction elements for benzodiazepine modulation of the GABA(A) receptor: three residues are required for allosteric coupling. *J Neurosci* **19**, 10213–10220 (1999).
84. Bera, A. K., Chatav, M. & Akabas, M. H. GABA(A) receptor M2-M3 loop secondary structure and changes in accessibility during channel gating. *J Biol Chem* **277**, 43002–43010 (2002).
85. Kash, T. L., Jenkins, A., Kelley, J. C., Trudell, J. R. & Harrison, N. L. Coupling of agonist binding to channel gating in the GABA(A) receptor. *Nature* **421**, 272–275 (2003).
86. Absalom, N. L., Lewis, T. M., Kaplan, W., Pierce, K. D. & Schofield, P. R. Role of charged residues in coupling ligand binding and channel activation in the extracellular domain of the glycine receptor. *J Biol Chem* **278**, 50151–50157 (2003).
87. Scott, S., Lynch, J. W. & Keramidis, A. Correlating structural and energetic changes in glycine receptor activation. *J Biol Chem* **290**, 5621–5634 (2015).
88. Lummis, S. C. *et al.* Cis-trans isomerization at a proline opens the pore of a neurotransmitter-gated ion channel. *Nature* **438**, 248–252 (2005).
89. Reeves, D. C., Jansen, M., Bali, M., Lemster, T. & Akabas, M. H. A role for the beta 1-beta 2 loop in the gating of 5-HT<sub>3</sub> receptors. *J Neurosci* **25**, 9358–9366 (2005).
90. Paulsen, I. M., Martin, I. L. & Dunn, S. M. Isomerization of the proline in the M2-M3 linker is not required for activation of the human 5-HT<sub>3A</sub> receptor. *J Neurochem* **110**, 870–878 (2009).
91. Jha, A., Cadugan, D. J., Purohit, P. & Auerbach, A. Acetylcholine receptor gating at extracellular transmembrane domain interface: the cys-loop and M2-M3 linker. *J Gen Physiol* **130**, 547–558 (2007).
92. Lee, W. Y., Free, C. R. & Sine, S. M. Binding to gating transduction in nicotinic receptors: Cys-loop energetically couples to pre-M1 and M2-M3 regions. *J Neurosci* **29**, 3189–3199 (2009).
93. Wiltfong, R. E. & Jansen, M. Probing protein packing surrounding the residues in and flanking the nicotinic acetylcholine receptor M2M3 loop. *J Neurosci* **29**, 1626–1635 (2009).
94. Sala, E., Mulet, J., Sala, S., Gerber, S. & Criado, M. Charged amino acids of the N-terminal domain are involved in coupling binding and gating in alpha7 nicotinic receptors. *J Biol Chem* **280**, 6642–6647 (2005).
95. Law, R. J., Henchman, R. H. & McCammon, J. A. A gating mechanism proposed from a simulation of a human alpha7 nicotinic acetylcholine receptor. *Proc Natl Acad Sci USA* **102**, 6813–6818 (2005).
96. Zhang, J. *et al.* Desensitization of alpha7 nicotinic receptor is governed by coupling strength relative to gate tightness. *J Biol Chem* **286**, 25331–25340 (2011).
97. Grutter, T. *et al.* Molecular tuning of fast gating in pentameric ligand-gated ion channels. *Proc Natl Acad Sci USA* **102**, 18207–18212 (2005).
98. Bouzat, C., Bartos, M., Corradi, J. & Sine, S. M. The interface between extracellular and transmembrane domains of homomeric Cys-loop receptors governs open-channel lifetime and rate of desensitization. *J Neurosci* **28**, 7808–7819 (2008).
99. Couturier, S. *et al.* A neuronal nicotinic acetylcholine receptor subunit (alpha 7) is developmentally regulated and forms a homo-oligomeric channel blocked by alpha-BTX. *Neuron* **5**, 847–856 (1990).
100. Revah, F. *et al.* Mutations in the channel domain alter desensitization of a neuronal nicotinic receptor. *Nature* **353**, 846–849 (1991).
101. Peng, X., Katz, M., Gerzanich, V., Anand, R. & Lindstrom, J. Human alpha 7 acetylcholine receptor: cloning of the alpha 7 subunit from the SH-SY5Y cell line and determination of pharmacological properties of native receptors and functional alpha 7 homomers expressed in *Xenopus* oocytes. *Mol Pharmacol* **45**, 546–554 (1994).
102. Halevi, S. *et al.* The *C. elegans* ric-3 gene is required for maturation of nicotinic acetylcholine receptors. *EMBO J* **21**, 1012–1020 (2002).
103. Halevi, S. *et al.* Conservation within the RIC-3 gene family. Effectors of mammalian nicotinic acetylcholine receptor expression. *J Biol Chem* **278**, 34411–34417 (2003).
104. Gay, E. A., Giniatullin, R., Skorinkin, A. & Yakel, J. L. Aromatic residues at position 55 of rat alpha7 nicotinic acetylcholine receptors are critical for maintaining rapid desensitization. *J Physiol* **586**, 1105–1115 (2008).
105. Roncarati, R. *et al.* Functional properties of alpha7 nicotinic acetylcholine receptors co-expressed with RIC-3 in a stable recombinant CHO-K1 cell line. *Assay Drug Dev Technol* **6**, 181–193 (2008).
106. Andersen, N., Corradi, J., Sine, S. M. & Bouzat, C. Stoichiometry for activation of neuronal alpha7 nicotinic receptors. *Proc Natl Acad Sci USA* **110**, 20819–20824 (2013).
107. Andersen, N. D. *et al.* Exploring the positive allosteric modulation of human alpha7 nicotinic receptors from a single-channel perspective. *Neuropharmacology* **107**, 189–200 (2016).
108. Yan, H. *et al.* The coupling interface and pore domain codetermine the single-channel activity of the alpha7 nicotinic receptor. *Neuropharmacology* **95**, 448–458 (2015).
109. Collins, T., Young, G. T. & Millar, N. S. Competitive binding at a nicotinic receptor transmembrane site of two alpha7-selective positive allosteric modulators with differing effects on agonist-evoked desensitization. *Neuropharmacology* **61**, 1306–1313 (2011).
110. Wang, J., Horenstein, N. A., Stokes, C. & Papke, R. L. Tethered agonist analogs as site-specific probes for domains of the human alpha7 nicotinic acetylcholine receptor that differentially regulate activation and desensitization. *Mol Pharmacol* **78**, 1012–1025 (2010).
111. Karlsson, U., Druzin, M. & Johansson, S. Cl<sup>-</sup> concentration changes and desensitization of GABA(A) and glycine receptors. *J Gen Physiol* **138**, 609–626 (2011).
112. Hille, B. *Ion channels of excitable membranes*. (Sinauer Associates, Inc., 2001).
113. Ochoa, E. L., Li, L. & McNamee, M. G. Desensitization of central cholinergic mechanisms and neuroadaptation to nicotine. *Mol Neurobiol* **4**, 251–287 (1990).
114. Pidoplichko, V. L., DeBiasi, M., Williams, J. T. & Dani, J. A. Nicotine activates and desensitizes midbrain dopamine neurons. *Nature* **390**, 401–404 (1997).
115. Paradiso, K. G. & Steinbach, J. H. Nicotine is highly effective at producing desensitization of rat alpha4beta2 neuronal nicotinic receptors. *J Physiol* **553**, 857–871 (2003).
116. Giniatullin, R., Nistri, A. & Yakel, J. L. Desensitization of nicotinic ACh receptors: shaping cholinergic signaling. *Trends Neurosci* **28**, 371–378 (2005).
117. Nelson, M. E. & Lindstrom, J. Single channel properties of human alpha3 AChRs: impact of beta2, beta4 and alpha5 subunits. *J Physiol* **516** (Pt 3), 657–678 (1999).
118. Wu, J. *et al.* Roles of nicotinic acetylcholine receptor beta subunits in function of human alpha4-containing nicotinic receptors. *J Physiol* **576**, 103–118 (2006).

119. Zhao, L. *et al.* Functional properties of homomeric, human alpha 7-nicotinic acetylcholine receptors heterologously expressed in the SH-EP1 human epithelial cell line. *J Pharmacol Exp Ther* **305**, 1132–1141 (2003).
120. Martin, R. J. & Kusel, J. R. On the distribution of a fluorescent ivermectin probe (4'' 5,7 dimethyl-bodipy propionylivermectin) in *Ascaris* membranes. *Parasitology* **104** (Pt 3), 549–555 (1992).
121. Warnock, D. E. *et al.* Determination of plasma membrane lipid mass and composition in cultured Chinese hamster ovary cells using high gradient magnetic affinity chromatography. *J Biol Chem* **268**, 10145–10153 (1993).
122. Oehler, D. D. & Miller, J. A. Liquid chromatographic determination of ivermectin in bovine serum. *J Assoc Off Anal Chem* **72**, 59 (1989).
123. Etter, A. *et al.* PicROTOXIN blockade of invertebrate glutamate-gated chloride channels: subunit dependence and evidence for binding within the pore. *J Neurochem* **72**, 318–326 (1999).
124. Eisele, J. L. *et al.* Chimaeric nicotinic-serotonergic receptor combines distinct ligand binding and channel specificities. *Nature* **366**, 479–483 (1993).
125. Figl, A., Labarca, C., Davidson, N., Lester, H. A. & Cohen, B. N. Voltage-jump relaxation kinetics for wild-type and chimeric beta subunits of neuronal nicotinic receptors. *J Gen Physiol* **107**, 369–379 (1996).
126. Bouzat, C. *et al.* Coupling of agonist binding to channel gating in an ACh-binding protein linked to an ion channel. *Nature* **430**, 896–900 (2004).
127. Paas, Y. *et al.* Pore conformations and gating mechanism of a Cys-loop receptor. *Proc Natl Acad Sci USA* **102**, 15877–15882 (2005).
128. Pittel, I., Witt-Kehati, D., Degani-Katzav, N. & Paas, Y. Probing pore constriction in a ligand-gated ion channel by trapping a metal ion in the pore upon agonist dissociation. *J Biol Chem* **285**, 26519–26531 (2010).
129. Schmandt, N. *et al.* A chimeric prokaryotic pentameric ligand-gated channel reveals distinct pathways of activation. *J Gen Physiol* **146**, 323–340 (2015).
130. Chang, C. S., Olcese, R. & Olsen, R. W. A single M1 residue in the beta2 subunit alters channel gating of GABAA receptor in anesthetic modulation and direct activation. *J Biol Chem* **278**, 42821–42828 (2003).
131. Hu, X. Q., Zhang, L., Stewart, R. R. & Weight, F. F. Arginine 222 in the pre-transmembrane domain 1 of 5-HT3A receptors links agonist binding to channel gating. *J Biol Chem* **278**, 46583–46589 (2003).
132. Perkins, D. I. *et al.* Loop 2 Structure in Glycine and GABAA Receptors Plays a Key Role in Determining Ethanol sensitivity *J Biol Chem* **284**, 27304–27314 (2009).
133. Yamodo, I. H., Chiara, D. C., Cohen, J. B. & Miller, K. W. Conformational changes in the nicotinic acetylcholine receptor during gating and desensitization. *Biochemistry* **49**, 156–165 (2010).
134. Pless, S. A., Leung, A. W., Galpin, J. D. & Ahern, C. A. Contributions of conserved residues at the gating interface of glycine receptors. *J Biol Chem* **286**, 35129–35136 (2011).
135. Gonzalez-Gutierrez, G., Cuello, L. G., Nair, S. K. & Grosman, C. Gating of the proton-gated ion channel from *Gloeobacter violaceus* at pH 4 as revealed by X-ray crystallography. *Proc Natl Acad Sci USA* **110**, 18716–18721 (2013).
136. Bertozzi, C., Zimmermann, I., Engeler, S., Hilf, R. J. & Dutzler, R. Signal Transduction at the Domain Interface of Prokaryotic Pentameric Ligand-Gated Ion Channels. *PLoS Biol* **14**, e1002393 (2016).
137. Lynagh, T., Webb, T. I., Dixon, C. L., Cromer, B. A. & Lynch, J. W. Molecular determinants of ivermectin sensitivity at the glycine receptor chloride channel. *J Biol Chem* **286**, 43913–43924 (2011).
138. Hernando, G. & Bouzat, C. *Caenorhabditis elegans* neuromuscular junction: GABA receptors and ivermectin action. *PLoS One* **9**, e95072 (2014).
139. Cheng, Y. & Prusoff, W. H. Relationship between the inhibition constant (K1) and the concentration of inhibitor which causes 50 per cent inhibition (I50) of an enzymatic reaction. *Biochem Pharmacol* **22**, 3099–3108 (1973).
140. Du, J., Lu, W., Wu, S., Cheng, Y. & Gouaux, E. Glycine receptor mechanism elucidated by electron cryo-microscopy. *Nature* **526**, 224–229 (2015).

## Acknowledgements

This work was supported by the Wolfson Family Foundation and the Israel Science Foundation who granted the equipment used in this study.

## Author Contributions

N.D.-K. and Y.P. designed the study; N.D.-K., M.K., M.H.-E., R.G., R.T. and Y.P. performed research and analyzed data; N.D.-K. and Y.P. wrote the paper.

## Additional Information

**Supplementary information** accompanies this paper at <http://www.nature.com/srep>

**Competing financial interests:** The authors declare no competing financial interests.

**How to cite this article:** Degani-Katzav, N. *et al.* Trapping of ivermectin by a pentameric ligand-gated ion channel upon open-to-closed isomerization. *Sci. Rep.* **7**, 42481; doi: 10.1038/srep42481 (2017).

**Publisher's note:** Springer Nature remains neutral with regard to jurisdictional claims in published maps and institutional affiliations.



This work is licensed under a Creative Commons Attribution 4.0 International License. The images or other third party material in this article are included in the article's Creative Commons license, unless indicated otherwise in the credit line; if the material is not included under the Creative Commons license, users will need to obtain permission from the license holder to reproduce the material. To view a copy of this license, visit <http://creativecommons.org/licenses/by/4.0/>

© The Author(s) 2017